Many-Body Localization in the Massless Schwinger Model

by Ahmed Akhtar
Advisor: Prof. Shivaji Sondhi
Co-Advisor: Dr. Mari Carmen Bañuls

A senior thesis
submitted to the Department of Physics
in partial fulfillment of the requirements
for the degree of Bachelor of the Arts

Princeton University
Princeton, New Jersey

May 1, 2017

Contents

Acknowledgments

Thanks to

Professor Sondhi, who helped me every step of the way and without whom this thesis would not have come to fruition.

Dr Mari Carmen, who was an invaluable mentor throughout this process.

Professor Rahul Nandkishore, who guided the numerics.

Sumit Saluja, who set me up on the Feynman Cluster.

The Feynman Computing Cluster, without whom this thesis would not be possible.

My friends, especially Davis, Nathan, and Adam, for their time and insight, and Julia, for her support.

My parents, who I owe everything to.

For my new-born baby nephew, and, allegedly, the spitting-image of myself when I was born, Gabriel Ibrahim Blomquist.

Many-Body Localization in the Massless Schwinger Model

by Ahmed Akhtar

Abstract

The massless Schwinger model, a one-dimensional system of massless fermions with a long-range Coulombic interaction, is equivalent to a non-interacting bosonic field with a mass term in the bosonization regime. This begs the question: does the massless Schwinger model many-body localize upon the addition of disorder? We answer this question by calculating the level statistics ratio for the disordered massless Schwinger model in the low-interaction regime, where bosonization applies. Our results suggest that the system many-body localizes in the bosonization regime at low energy densities. We present numerical evidence from finite size studies of a lattice version of the model in support of this conclusion.

1 Introduction: The Schwinger Model

The Schwinger model is a 1+1 dimensional model for quantum electrodynamics. It describes the interaction of a fermionic Dirac field with an electric field, as there is no $\vec{B}$ field in only one spatial dimension. The Lagrangian density is given in terms of the vector two-potential $A_\mu = (A_0, A_1)$, the Maxwell tensor $F_{\mu\nu} = \partial_\mu A_\nu - \partial_\nu A_\mu$, the magnitude of the charge g, the mass m of the particles, the Dirac γ matrices and, of course, the two-component fermionic field Ψ [1].

$$\mathcal{L} = \bar{\Psi}(-i\gamma^\mu \partial_\mu + g\gamma^\mu A_\mu + m)\Psi + \frac{1}{4} F_{\mu\nu} F^{\mu\nu} \tag{1}$$

The model describes the interaction of a charged particle and its antiparticle on a line. Particle-antiparticle pairs can be created and destroyed, and each particle emits an electric field that is constant as a function of distance[1].

We can simplify the model by employing the temporal gauge condition, where there is zero scalar potential $A_0 = 0$. There are only two non-zero components of the Maxwell tensor, which in the temporal gauge becomes $F_{01} = \partial_0 A_1 = -F_{10}$. Recall that the electric field is given in terms of the potentials V and $\vec{A}$ by the relation $E = -\nabla V - \partial_t \vec{A}$. In 1+1 dimensions, and in the temporal gauge, this implies $E = -\partial_0 A_1$. Using this and the Minkowski metric with signature $(+,-)$, we can write $F_{\mu\nu}F^{\mu\nu}$ in terms of the electric field E.

$$F_{\mu\nu} = \begin{pmatrix} 0 & -E \\ E & 0 \end{pmatrix} \qquad F^{\mu\nu} = \begin{pmatrix} 0 & E \\ -E & 0 \end{pmatrix} \tag{2}$$

$$\mathcal{H} = \bar{\Psi}\gamma^1(-i\partial_1 - gA_1)\Psi + m\bar{\Psi}\Psi + \frac{1}{2}E^2 \tag{3}$$

The Schwinger model is the Dirac field with an added electric field [2]. To understand the various components of this formulation, we digress to a brief summary of the Dirac equation.

1.1 1+1D Dirac Equation with an Electric Field

Dirac came up with his equation when trying to describe the relativistic quantum realm. The equation is in terms of a set of symbols $\{\gamma^\mu\}$ which commute with the momentum operators and also obey anti-commutation relations $\{\gamma^\mu, \gamma^\nu\} = 2g^{\mu\nu}\mathbb{I}$, where $g_{\mu\nu}$ with signature $(+,-)$ is the Minkowski metric in 1+1d [3].

$$(-i\gamma^\mu \partial_\mu + m)\psi = 0 \tag{4}$$

[1] In the spin language, after the Hamiltonian is discretized, it is apparent that the particles interact via a linear potential that is proportional to the product of the charges (i.e. a one-dimensional Coulombic potential).

With these anti-commutation relations, plane waves $e^{ipx}\Psi_0$ satisfy the mass-shell condition $p^2 = m^2$. This is found by multiplying the above equation by the plane wave $e^{ip_\mu x^\mu}\Psi_0$, and then multiplying that by its complex conjugate, and then applying the anti-commutation relation.

In 1+1 dimensions, we can choose the γ matrices to be:

$$\gamma^0 = \begin{pmatrix} 0 & 1 \\ 1 & 0 \end{pmatrix} \qquad \gamma^1 = \begin{pmatrix} 0 & -1 \\ 1 & 0 \end{pmatrix} \tag{5}$$

Now that we have the form of the gamma matrices, we can solve for the energies of the free Dirac fermion. In analogy to non-relativistic quantum mechanics, we will make the correspondence $p \equiv -i\partial_x$. Rearranging the Dirac equation and multiplying both sides by γ^0 suggests the form of the Hamiltonian which can be diagonalized to find the spectrum of the free Dirac fermion.

$$-i\gamma^0\partial_t\psi = -m\psi - \gamma^1 p\psi \tag{6}$$

$$i\partial_t\psi = m\gamma^0\psi + \gamma^0\gamma^1 p\psi \tag{7}$$

$$i\partial_t\psi = \begin{pmatrix} p & m \\ m & -p \end{pmatrix}\psi \tag{8}$$

$$\implies H = \begin{pmatrix} p & m \\ m & -p \end{pmatrix} \tag{9}$$

Thus the Dirac fermion is a two-component field, and if decomposed in the energy eigen-basis consists of one component with positive energy and one with negative energy. We can always break up the fermion field into these components. Furthermore, we can see that the free Dirac fermion has no ground state, which presents a number of physical problems (such as a divergent partition function). Dirac's answer to this was the concept of the Dirac sea, where all the negative energy modes are already occupied. A excitation then means a hole in a negative energy mode or an occupation in a positive energy mode. The occupied positive mode is interpreted as an electron and the hole as a positron. With this interpretation, there is a ground state (the Dirac sea), and each excited state is formed by creating pairs of positrons and electrons [3].

$$E = \pm\sqrt{p^2 + m^2} \tag{10}$$

The last bit of information we need about the free Dirac fermion is the conserved quantities from the equation. Treating the field as a 2-vector, if we take the adjoint of the Dirac equation and multiply on the right by γ^0 we get a conservation equation for the current $J^\mu = \bar{\psi}\gamma^\mu\psi$, where $\bar{\psi} \equiv \psi^\dagger\gamma^0$.

$$i\partial_0\psi^\dagger + i\partial_1\psi^\dagger\gamma^0\gamma^1 + m\psi^\dagger\gamma^0 = 0 \tag{11}$$

$$i\partial_\mu\bar{\psi}\gamma^\mu + m\bar{\psi} = 0 \tag{12}$$

$$\implies \partial_\mu(\bar{\psi}\gamma^\mu\psi) = (\partial_\mu\bar{\psi}\gamma^\mu)\psi + \bar{\psi}(\gamma^\mu\partial_\mu\psi) = -\frac{m}{i}\bar{\psi}\psi + \frac{m}{i}\bar{\psi}\psi = 0 \tag{13}$$

The component $J^0 = \psi^\dagger\psi$ is referred to as the charge density in analogy to the conservation equation in electromagnetism. If total charge is conserved, its integral over all space is constant. Since electrons and positrons carry opposite sign, J^0 is the difference between the density of electrons and positrons [3].

Now that we are armed with a cursory understanding of the Dirac fermion, we can examine the Hamiltonian densities presented in the beginning of the chapter in analogy to the Hamiltonian for classical electrodynamics.

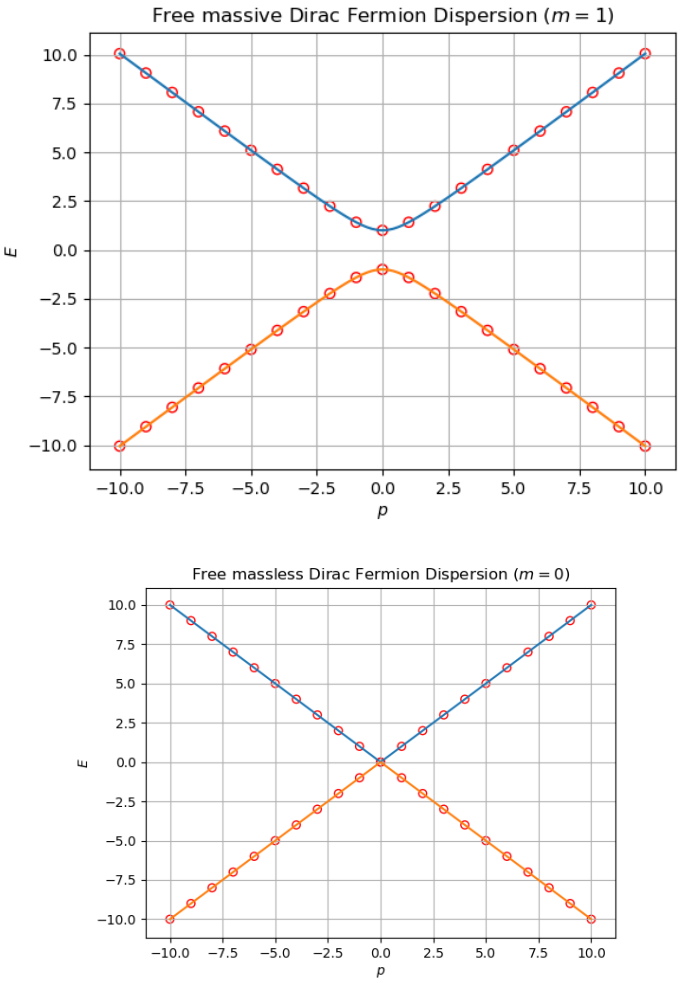

Figure 1: The graph on top represents the massive Dirac fermion, which has a gap between the positive and negative energy states. The circles represent discrete modes in a finite volume. The graph on bottom is the dispersion for the massless Dirac fermion. The figures in this section and others were generated using [4] or [5].

1.2 Analogy to the Hamiltonian for Classical Electrodynamics

To understand the Schwinger model, let's begin with the classical Lagrangian [6] for a particle in an electromagnetic field with vector potential $\vec{A} = (A_x, A_y, A_z)$ and scalar potential V in three spatial dimensions:

$$L(\vec{r}, \dot{\vec{r}}, t) = \frac{1}{2}m|\dot{\vec{r}}|^2 - q(V - \dot{\vec{r}} \cdot \vec{A}) \tag{14}$$

$$= \frac{1}{2}m(\dot{x}^2 + \dot{y}^2 + \dot{z}^2) - qV + q(\dot{x}A_x + \dot{y}A_y + \dot{z}A_z) \tag{15}$$

We can easily verify that this Lagrangian recovers the correct equation of motion (i.e. the Lorentz force law) by using the Euler-Lagrange equations. Recall that V and $\vec{A}$ are functions of the spatial coordinates and t only and that potentials are related to the fields by the equations $\vec{B} = \nabla \times \vec{A}$ and $\vec{E} = -\nabla V - \frac{\partial \vec{A}}{\partial t}$. The equation for the x-direction is $\frac{\partial L}{\partial x} = \frac{d}{dt}(\frac{\partial L}{\partial \dot{x}})$, and gives the x-component of the Lorentz force law. The reader can verify the remaining directions.

$$m\ddot{x} + q\frac{dA_x}{dt} = q(-\frac{\partial V}{\partial x} + \dot{\vec{r}} \cdot \frac{\partial \vec{A}}{\partial x}) \tag{16}$$

$$m\ddot{x} = q(-\frac{\partial V}{\partial x} + \dot{\vec{r}} \cdot \frac{\partial \vec{A}}{\partial x} - \frac{dA_x}{dt}) \tag{17}$$

$$= q(-\frac{\partial V}{\partial x} - \frac{\partial A_x}{\partial t} + \dot{y}(\frac{\partial A_y}{\partial x} - \frac{\partial A_x}{\partial y}) + \dot{z}(\frac{\partial A_z}{\partial x} - \frac{\partial A_x}{\partial z})) \tag{18}$$

$$= q(E_x + [\dot{\vec{r}} \times B]_x) \tag{19}$$

The corresponding conjugate momentum is $\vec{p} = m\dot{\vec{r}} + q\vec{A}$, which gives a Lagrangian and Hamiltonian in terms of these canonical variables.

$$L = \frac{1}{2m}|\vec{p} - q\vec{A}|^2 - q(V - \frac{1}{m}(\vec{p} - q\vec{A}) \cdot \vec{A}) = \frac{1}{2m}(|\vec{p}|^2 - q^2|\vec{A}|^2) - qV \tag{20}$$

$$H = \frac{1}{2m}|\vec{p} - q\vec{A}|^2 + qV \tag{21}$$

Comparing this to the Hamiltonian density $\mathcal{H} = \bar{\Psi}\gamma^1(-i\partial_x - gA_1)\Psi + m\bar{\Psi}\Psi + \frac{1}{2}E^2$ for the Schwinger model, and to the free Dirac Hamiltonian $H = m\gamma^0 + \gamma^0\gamma^1 p$, we see how different terms in each correspond. The Hamiltonian density for the Schwinger model includes terms for the free Dirac fermion in addition to terms for the electric field energy. We can now think of the Schwinger model as QED in 1+1 dimensions.

1.3 The Bosonized Massless Schwinger model

Bosonization is a way to translate a Hamiltonian written in terms of a fermion field, obeying a set of anti-commutation relations, into a Hamiltonian of a boson field obeying a set of commutation

$$\boxed{H = H_0^F + V \quad \rightarrow \text{bosonization} \rightarrow \quad H = H_0^B + V^B}$$

Figure 2: Via bosonization, the Hamiltonian on the left is converted to the one on the right. The free fermion field is mapped into a free boson field, and any perturbation is translated via the dictionary.

relations. It is often presented as a dictionary relating terms in fermion language to terms in boson language. Although bosonization only applies to Hamiltonians with linearized dispersion relations, it is particularly powerful in one-dimension. With it, we can solve a number of Hamiltonians with weak interactions by linearizing the dispersion relations near the Fermi points. We will show that each term in the massless Schwinger model translates to a term in the bosonized harmonic oscillator. The reader can refer to [7], [8] for details about the dictionary.

$$H = \int dx \left(\bar{\Psi} \gamma^1 (-i\partial_x - gA_1)\Psi + \frac{1}{2} E^2 \right) \tag{22}$$

The first part of the Hamiltonian maps to the free massless scalar field, H_B, which is given in terms of a (two-component) bosonic operator ϕ and its conjugate field Π as

$$\mathcal{H}_B \propto \Pi^2 + (\partial_x \phi)^2 \tag{23}$$

To bosonize the electric field term, we make use of the following identity relating the Maxwell tensor to the current density J^μ [2].

$$\partial_\nu F^{\nu\mu} = g J^\mu \tag{24}$$

Referring to the bosonization dictionary, we find that

$$J^\mu = \frac{1}{\sqrt{\pi}} \in^{\mu\nu} \partial_\nu \phi \tag{25}$$

Which gives $\partial_t E = -\frac{g}{\sqrt{\pi}} \partial_t \phi$ for $\mu = 1$. Thus, $E \propto \phi$, and so $E^2 \propto \phi^2$. The massless Schwinger model is equivalent to a massive non-interacting boson field theory, or similarly to a chain of coupled harmonic oscillators with a pinning term [1]. This equivalence is only valid when the interaction is weak and near the Fermi points.

The fact that the massless Schwinger model is equivalent to this boson model is crucial to the current study. It motivates the question, does the massless Schwinger model localize? In the fermion language, the obvious answer seems to be no, because it has long-range interactions [9]. However, in the boson language, the Hamiltonian can be diagonalized into a sum of number operators for each mode. It seems that in the boson language, it should localize.

2 The Schwinger Model on the Lattice

In this section, we explore the discretized Schwinger model. We show that the discretized Hamiltonian becomes the free Dirac fermion in the continuum limit when $A \to 0$. We also present an alternative choice of background charge that is not used in this thesis. Finally, we present the classical equivalent to the Schwinger model, the two-component Coulomb plasma.

2.1 Lattice Formulation of the Model

The Schwinger model can be discretized on a lattice. The Kogut-Susskind formulation of the Schwinger model is presented in [1] and can be learned in more detail in [10]. In this subsection, we will present the discretized Hamiltonian and show that it recovers the free Dirac fermion in limit of small momenta and energy.

There are N sites on the lattice, labeled $0...N-1$, and on each there sits a single component fermionic field operator ϕ_n. The lattice constant is a. Additionally, we define lattice variables θ_n and L_n, where L_n corresponds to the electric field E_n between site n and $n+1$. The full, discretized Hamiltonian is

$$H = \frac{-i}{2a}\sum_n(\phi_n^\dagger e^{i\theta_n}\phi_{n+1} - h.c.) + m\sum_n(-1)^n\phi_n^\dagger\phi_n + \frac{ag^2}{2}\sum_n L_n^2 \tag{26}$$

In the case of zero electric field, the Hamiltonian becomes

$$H = \frac{-i}{2a}\sum_n(\phi_n^\dagger\phi_{n+1} - h.c.) + m\sum_n(-1)^n\phi_n^\dagger\phi_n \tag{27}$$

The fermion field ϕ_n is the annihilation operator for site n i.e. it destroys a particle on site n. If we take the discrete Fourier transform of the field operators, we end up with another set of operators $c_k, c_k^\dagger$ which are also fermionic [11]. We interpret these operators as creation and annihilation operators in momentum-space ($\hbar = 1$). To ensure that we preserve the number of degrees of freedom, we will require that different values of k differ by integer multiples of $2\pi/N$, which gives N linearly independent operators. This also makes the momentum-space fermionic operators periodic, and so $c_k = c_{k+2\pi}$ or equivalently $c_{k-\pi} = c_{k+\pi}$. Note that in making the momentum-space operators periodic, we have also made the original fermionic operators periodic i.e. $\phi_0 = \phi_N$. Thus, in what follows, we will consider periodic boundary conditions and allow hopping from site 0 to site $N-1$ and vice versa.

$$c_k \equiv \frac{1}{\sqrt{N}}\sum_{n=0}^{N-1} e^{-ikn}\phi_n \quad \iff \quad \phi_n = \frac{1}{\sqrt{N}}\sum_k e^{ikn}c_k \qquad k = 2\pi q/N \quad q \in \{0...N-1\} \tag{28}$$

$$\begin{aligned}\{c_k, c_{k'}\} &= \{\frac{1}{\sqrt{N}}\sum_{n=0}^{N-1} e^{-ikn}\phi_n, \frac{1}{\sqrt{N}}\sum_{n'=0}^{N-1} e^{-ik'n'}\phi_{n'}\} \\ &= \frac{1}{N}\sum_{n,n'=0}^{N-1} e^{-i(kn+k'n')}\{\phi_n, \phi_{n'}\} \\ &= 0 = \{c_k^\dagger, c_{k'}^\dagger\}\end{aligned}$$

$$\begin{aligned}\{c_k, c_{k'}^\dagger\} &= \{\frac{1}{\sqrt{N}}\sum_{n=0}^{N-1} e^{-ikn}\phi_n, \frac{1}{\sqrt{N}}\sum_{n'=0}^{N-1} e^{ik'n'}\phi_{n'}^\dagger\} \\ &= \frac{1}{N}\sum_{n,n'=0}^{N-1} e^{i(-kn+k'n')}\{\phi_n, \phi_{n'}^\dagger\} = \frac{1}{N}\sum_{n,n'=0}^{N-1} e^{i(-kn+k'n')}\delta_{n,n'} \\ &= \frac{1}{N}\sum_{n=0}^{N-1} e^{in(k'-k)} = \delta_{k,k'}\end{aligned}$$

$$\{c_k, c_{k'}\} = \{c_k^\dagger, c_{k'}^\dagger\} = 0 \qquad \{c_k, c_{k'}^\dagger\} = \delta_{k,k'} \qquad c_{k-\pi} = c_{k+\pi} \tag{29}$$

To find the dispersion relation of this model, we can now plug in the Fourier-transformed operators. We will see that the first term will become diagonal in momentum-space, which makes finding the dispersion relation easier. This phenomenon is common for operators with "hopping" terms. This first term is called a hopping because when $\phi_n^\dagger\phi_{n+1}$ acts on a site, it destroys a particle on site $n+1$ and creates one on n, hopping the particle one site over.

Furthermore, in what follows we will assume N is even. This is required to have periodicity in the system, since the discretized Hamiltonian has an on-site potential that repeats every two sites. In order to preserve this symmetry, we cannot have N be odd.

$$\begin{aligned}H_{hop} &= \frac{-i}{2a}\sum_{n=0}^{N-1} \phi_n^\dagger\phi_{n+1} - \phi_{n+1}^\dagger\phi_n \\ &= \frac{-i}{2aN}\sum_{n=0}^{N-1}\sum_{k,k'} e^{-ikn}e^{ik'(n+1)}c_k^\dagger c_{k'} - e^{-ik'(n+1)}e^{ikn}c_{k'}^\dagger c_k \\ &= \frac{-i}{2aN}\sum_{k,k'}(\sum_{n=0}^{N-1} e^{in(k'-k)})e^{ik'}c_k^\dagger c_{k'} - (\sum_{n=0}^{N-1} e^{in(k-k')})e^{-ik'}c_{k'}^\dagger c_k \\ &= \frac{-i}{2a}\sum_k e^{ik}c_k^\dagger c_k - e^{-ik}c_k^\dagger c_k\end{aligned}$$

$$
\begin{aligned}
H_{pot} &= m\sum_{n=0}^{N-1} e^{i\pi n}\phi_n^\dagger\phi_n = \frac{m}{N}\sum_{n,k,k'} e^{i\pi n}e^{-ikn}e^{ik'n}c_k^\dagger c_{k'} \\
&= \frac{m}{N}\sum_{n,k,k''} e^{-ikn}e^{ik''n}c_k^\dagger c_{k''-\pi} \\
&= \frac{m}{N}\sum_{k,k''}(\sum_n e^{in(k''-k)})c_k^\dagger c_{k''-\pi} \\
&= m\sum_k c_k^\dagger c_{k+\pi}
\end{aligned}
$$

$$
H = \frac{1}{a}\sum_k(\sin k)c_k^\dagger c_k + m\sum_k c_k^\dagger c_{k+\pi} \tag{30}
$$

We have a choice over where to sum over k, and in the continuum limit this becomes the choice of where to integrate over k. Let's suppose that in the continuum limit we integrate k over the interval $[-\pi,\pi]$. Then, because of the symmetry in $\sin k$, we can re-write the integral as a sum of two integrals over the interval $[-\pi/2,\pi/2]$. These two integrals will be the branches that we associate with the free Dirac fermion dispersion relation.

$$
\begin{aligned}
H_{hop} &\propto \int_{-\pi}^{\pi}(\sin k)c_k^\dagger c_k dk \\
&= \int_{-\pi/2}^{\pi/2}(\sin k)c_k^\dagger c_k dk + \int_{-\pi/2}^{\pi/2}(\sin(k+\pi))c_{k+\pi}^\dagger c_{k+\pi}dk \\
&= \int_{-\pi/2}^{\pi/2}(\sin k)c_k^\dagger c_k - (\sin k)c_{k+\pi}^\dagger c_{k+\pi}dk
\end{aligned}
$$

$$
H_{pot} \propto \int_{-\pi}^{\pi} mc_k^\dagger c_{k+\pi}dk = \int_{-\pi/2}^{\pi/2} mc_k^\dagger c_{k+\pi}dk + \int_{-\pi/2}^{\pi/2} mc_{k+\pi}^\dagger c_k dk
$$

Thus, in the continuum limit we see that Hamiltonian goes to

$$
H \rightarrow_{N\rightarrow\infty,a\rightarrow 0} \int_{-\pi/2}^{\pi/2}\begin{pmatrix}c_k^\dagger & c_{k+\pi}^\dagger\end{pmatrix}\begin{pmatrix}\sin k & m \\ m & -\sin k\end{pmatrix}\begin{pmatrix}c_k \\ c_{k+\pi}\end{pmatrix}dk \tag{31}
$$

Finally, in the low-momentum limit, we retrieve the free Dirac Hamiltonian. We see that $c_{k+\pi}, c_{k+\pi}^\dagger$ represent the fermionic operators for the branch with negative slope in the free Dirac fermion spectrum. They correspond to particles who have positive energy when their momentum is negative, and negative energy when their momentum is positive. Consequently, they are referred to as *left-movers* and the other branch is referred to as *right-movers* [3].

$$
H \rightarrow_{N\rightarrow\infty,a\rightarrow 0,k<<1} \int_{-\pi/2}^{\pi/2}\begin{pmatrix}c_k^\dagger & c_{k+\pi}^\dagger\end{pmatrix}\begin{pmatrix}k & m \\ m & -k\end{pmatrix}\begin{pmatrix}c_k \\ c_{k+\pi}\end{pmatrix}dk \tag{32}
$$

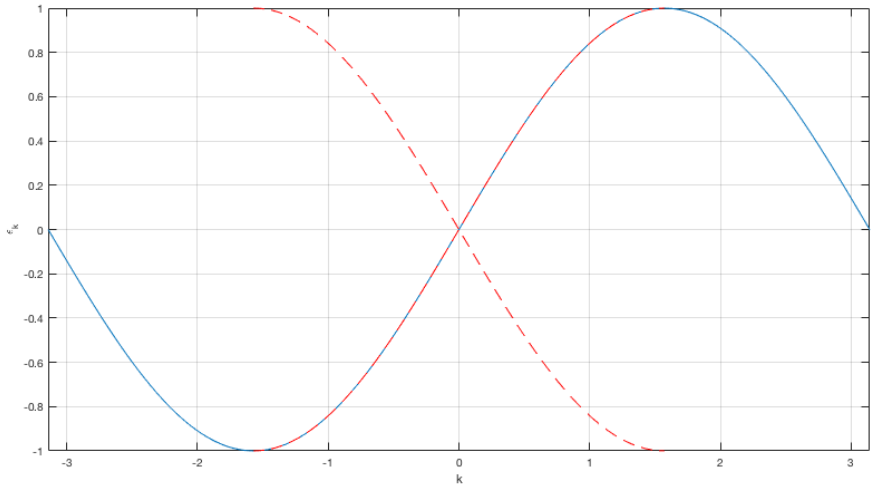

Figure 3: The red-dashed lines are the dispersion relation for the continuum-limit of the discretized Schwinger model.

2.2 Converting to Spin Language

We begin with a slightly modified form of the lattice Schwinger model [1]. First, we will be restricting ourselves to the massless case, since the system bosonizes in this case. Additionally, we re-scale the Hamiltonian by a factor of $\frac{2}{ag^2}$.

$$H = \frac{-i}{a^2 g^2} \sum_n (\phi_n^\dagger e^{i\theta_n} \phi_{n+1} - h.c.) + \sum_n L_n^2 \tag{33}$$

The lattice formulation suggests a form of Gauss's law where L_n acts as the field between sites n and $n+1$. Recall that the local charge density in the continuum Schwinger model can be positive, negative, or zero. Since we have a single component fermion field ϕ_n on each site, the local density operator $\phi_n^\dagger \phi_n$ can only take two values: 0 or 1. Thus, how do we recover the picture we presented in the beginning of this section of two types of particles, one of positive charge and one of negative charge. On each site, we should be allowed to have a charge of 0 if there is no particle, 1 if there is a positron and -1 if there is an electron.

$$L_n - L_{n-1} = \phi_n^\dagger \phi_n - \frac{1}{2}(1 - (-1)^n) \tag{34}$$

This picture is realized by a staggered background charge density of -1 on odd sites, and 0 on

Figure 4: The picture for the lattice Schwinger model.

Table 1: Allowed values for the charge on site n.

$\rho(n)$	unoccupied	occupied
n even	0	1
n odd	-1	0

even sites. Then the total background charge density $\phi_n^\dagger\phi_n - \frac{1}{2}(1-(-1)^n)$ can take the values 0, 1 on even sites, and -1, 0 on odd sites. This suggests that positrons inhabit even sites, and electrons inhabit odd sites.

We can use the recurrence relation from Gauss's Law to solve for the field in terms of the fermionic operators. If we use l_0 to denote the field to the left of site 0, then we can re-write the $\sum L_n^2$ term in terms of local spin operators σ_n^z and parameter l_0 using the Jordan-Wigner transformation [12], $\phi_n \to \prod_{m<n}(i\sigma_m^z)\sigma_n^-$.

$$L_n = l_0 + \sum_{k=0}^{n}\phi_k^\dagger\phi_k - \frac{1}{2}\sum_{k=0}^{n}(1-(-1)^k) \tag{35}$$

$$\phi_k^\dagger\phi_k \to = (\prod_{m<k}(i\sigma_m^z)\sigma_k^-)^\dagger(\prod_{m<k}(i\sigma_m^z)\sigma_k^-) = \sigma_k^+\sigma_k^- = \frac{1}{2}(\sigma_k^z+1)$$

$$L_n = l_0 + \frac{1}{2}\sum_{k=0}^{n}\left(\sigma_k^z + (-1)^k\right) \tag{36}$$

Note that l_0 is a function of the total charge in the system and some background field α generated by two far-away charges. It is only a valid parameter in some S_{total}^z eigenspace. If we are working in a system with charge conservation, or equivalently, if we are working in the fixed sector of S_{total}^z, and the background field is fixed, then the value of l_0 is constant. We could also re-write the Hamiltonian in terms of the physically significant parameter α. Since l_0 is simply the total field to the left of the system, it is related to α by $l_0 = \alpha - \frac{1}{2}Q_{total}$.

$$\begin{aligned} l_0 &= \alpha - \frac{1}{2}\sum_{n=0}^{N-1}\left(\phi_n^\dagger\phi_n - \frac{1}{2}(1-(-1)^n)\right) \\ &= \alpha - \frac{1}{2}\sum_{n=0}^{N}\left(\frac{1}{2}(\sigma_n^z+1) - \frac{1}{2}(1-(-1)^n)\right) \\ &= \alpha - \frac{1}{4}\sum_{n=0}^{N-1}\sigma_n^z \end{aligned}$$

$$L_n = \alpha + \frac{1}{4}\left(\sum_{k=0}^{n}\sigma_k^z - \sum_{k=n+1}^{N-1}\sigma_k^z\right) + \frac{1}{2}\sum_{k=0}^{n}(-1)^k \tag{37}$$

We are interested in the Schwinger model in the case where the total charge is zero, or $S_{total}^z = 0$. In this case, $l_0 = \alpha$. We define $x \equiv \frac{1}{g^2a^2}$, and we introduce the parameter λ to represent the strength

of the interaction. Then, the massless, lattice Schwinger Hamiltonian (with net-zero charge) can be represented in the spin language with parameters N, l_0, x, λ:

$$H = x \sum_{n=0}^{N-2} \left(\sigma_n^+ \sigma_{n+1}^- + \sigma_n^- \sigma_{n+1}^+\right) + \lambda \sum_{n=0}^{N-2} \left(l_0 + \frac{1}{2} \sum_{k=0}^{n} \left(\sigma_k^z + (-1)^k\right)\right)^2 \tag{38}$$

To program this, we need to pick a basis. If the local basis states are ordered by $|1\rangle, |0\rangle$ where $|1\rangle$ is the eigenvector of σ^z with eigenvalue +1, and the other has eigenvalue -1, then the total basis is ordered $|1...1\rangle$, $|1...0\rangle$, $...|0...0\rangle$. The Hamiltonian is block-diagonal in this basis. This is clear because $[H, S^z_{total}] = 0$. We can prove this directly. The hopping term is the only non-trivial part of this demonstration, thus we will only focus on it. We will apply the identities $[\sigma^+, \sigma^z] = -2\sigma^+$, $[\sigma^-, \sigma^z] = 2\sigma^-$.

$$\begin{aligned}
[\sum_{n=0}^{N-2} \left(\sigma_n^+ \sigma_{n+1}^- + \sigma_n^- \sigma_{n+1}^+\right), \sum_{k=0}^{N-1} \sigma_k^z] &= \sum_{n=0}^{N-2} (\sum_{k=0}^{N-1} [\sigma_n^+ \sigma_{n+1}^-, \sigma_k^z]) + (\sum_{k=0}^{N-1} [\sigma_n^- \sigma_{n+1}^+, \sigma_k^z]) \\
&= 2 \sum_{n=0}^{N-2} -\sigma_n^+ \sigma_{n+1}^- + \sigma_n^+ \sigma_{n+1}^- + \sigma_n^- \sigma_{n+1}^+ - \sigma_n^- \sigma_{n+1}^+ = 0
\end{aligned}$$

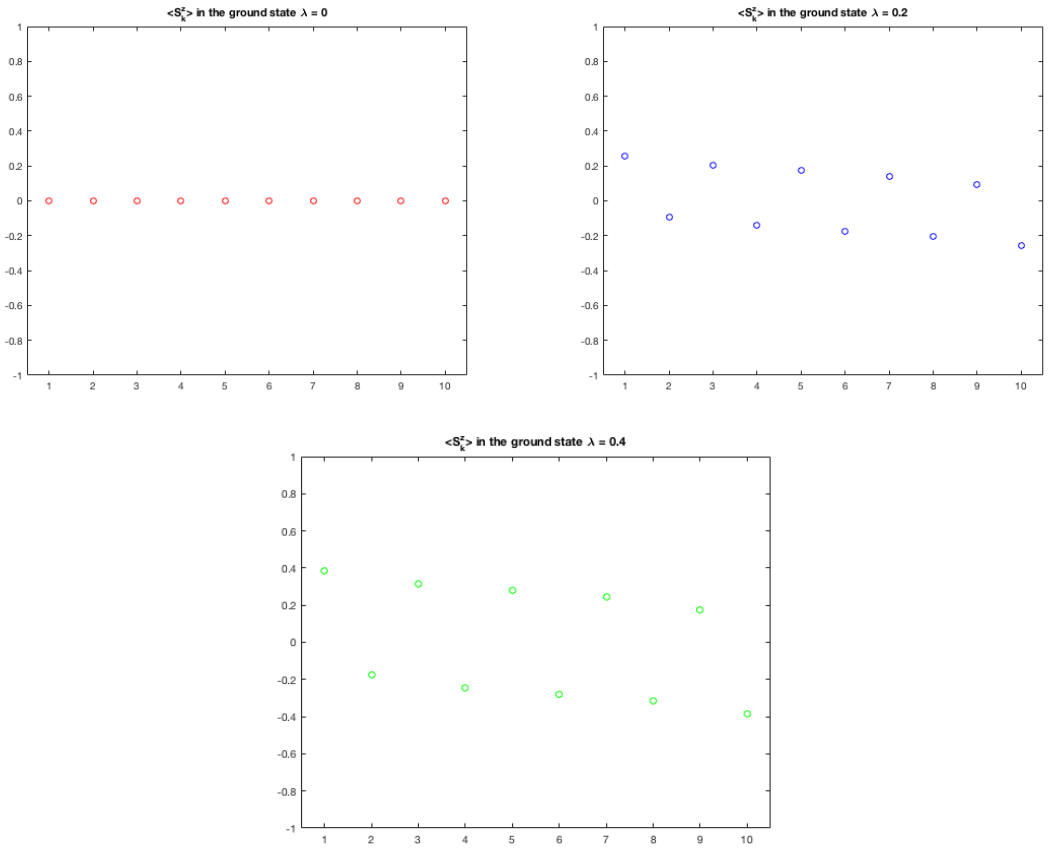

Figure 5: Here we show some numerical results of the model without disorder. In the ground state, to minimize the field L_n, we expect even sites to be unoccupied and odd sites to be occupied. In the spin language, this corresponds to $\sigma^z = -1$ for even sites, and $+1$ for odd sites. However, since this particular set of graphs is implemented in Matlab, index numbering starts at 1 and not 0. Therefore, we expect the reverse. Nonetheless, as we increase interaction strength λ, we see the crystalline structure become more defined.

2.3 Choices of Lattice Versions

If we choose a constant background charge, we get an alternative formulation of the Schwinger model with different physics. Suppose that instead of an alternating background charge, we used a constant background charge of $-\frac{1}{2}$. Gauss's Law in this model is somewhat simpler, and we can again solve for the field L_n at site n in terms of l_0, the field to the left of site 0. We use the notation in [1].

$$L_n - L_{n-1} = \phi_n^\dagger \phi_n - \frac{1}{2} \tag{39}$$

$$L_n = l_0 + \sum_{k=0}^{n} \phi_k^\dagger \phi_k - \frac{1}{2}(n+1) \tag{40}$$

We use Jordan-Wigner again to get the energy in the field.

$$\sum_n L_n^2 = \sum_n \left(l_0 + \frac{1}{2} \sum_{k=0}^{n} \sigma_k^z \right)^2 \tag{41}$$

If we consider Gauss's law for the entire system, we get L_n in terms of a background field α.

$$\sum_n L_n^2 = \sum_n \left(\alpha + \frac{1}{4} (\sum_{k=0}^{n} \sigma_k^z - \sum_{k=n+1}^{N-1} \sigma_k^z) \right)^2 \tag{42}$$

Although this model looks promising, there are only two options for the charge on a given site, $\pm\frac{1}{2}$. Thus, this model describes an entirely different set of physics. Namely, it cannot describe electrons and positrons creating and annihilating each other on a line. Rather, it makes more sense to interpret this model as *one* type of particle that can pop in and out of existence on a line of opposite charge. If there is no background field α, and $l_0 = 0$, the system is constrained to the $\sum_n \sigma_n^z = 0$ subspace. In this case, the model describes a fixed number of positive particles interacting on top of a constant negative charge density.

We ultimately used the model with an alternating background charge because it recovered the desired continuum physics. However, that different choices for the background charge can be so transformative on the physics raises many interesting questions. The two-component Coulomb plasma is the classical version of the model we focus on in this paper, while the one-component Coulomb plasma is the classical equivalent of the model we introduced in this section. They behave very differently at high temperature.

2.4 The Two-Component Coulomb Plasma

The two-component Coulomb plasma is a one-dimensional model for charged particle interactions. It is the naive classical equivalent to the Schwinger model. There are two popular models for the physics of Coulomb-interacting particles in 1D: jellium, or the one-component Coulomb plasma, can be understood as particles of one specie and charge interacting against a background of uniform and opposite charge; and the two-component Coulomb plasma, which can be pictured as a *two* different

species interacting under a linear potential [13]. We can think of the two-component plasma as one-dimensional electrodynamics. The potential energy of this model as a function of a background field $\theta = 2q$ (generated from charges q and $-q$ at the ends of the system) and system size L is

$$U_{L,\theta} = -e^2 \sum_{i<j}^{N} \sigma_i \sigma_j |x_i - x_j| - 2qe \sum_{i=1}^{N} \sigma_i x_i + q^2 L \tag{43}$$

where $\sigma_i \in \{-1, +1\}$, $x_i \in (0, L)$ represent the charge parity and position of particle i, respectively. Note that e, which is the charge of the particles in the system, is to be distinguished from q, which is the charge on the boundaries.

The first term is the potential between charges in the system. As we can see, the potential is minimized when opposite charges are close together and equal charges are far apart. The second term is the potential of each particle in the field θ, and as expected, potential is minimized when positive particles are farther upstream. The third term is the potential between the charges at the ends of the system, which have fixed position.

2.4.1 Preliminary physical properties of the model

We want to determine the electric field generated by a point charge. Imagine fixing such a charge σ_i at position x_i and imagine placing a positive test charge at position x_j. The electric potential of this system is given by

$$V = e|x_i - x_j| \tag{44}$$

By analogy to the electric field in 3-d, we get the electric field by differentiating V w.r.t. x_j, since $\Delta V = -E\Delta x = \frac{\Delta V}{\Delta x}\Delta x$.

$$E = -\frac{dV}{dx} = \begin{cases} -e & x_j < x_i \\ e & x_j > x_i \end{cases} \tag{45}$$

Thus, for a system of N particles, the field at x only depends on the number and species of the charges to the left and to the right. This is because the field is not a function of the distance as it is in 3-d.

$$E(x) = \int_0^L dy \, (\rho(y) sg(x - y)) \tag{46}$$

where $\rho(x) = \sum_i e\sigma_i \delta(x - x_i)$, $sg(x) = +1$ (-1) if $x > 0$ (if $x < 0$).

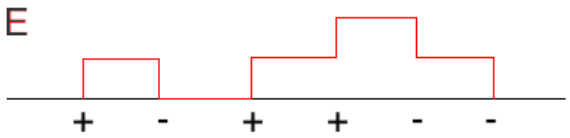

Figure 6: The E-field is only a function of how much charge is to the left or to the right of each link.

$$E(x) = \int_0^L dy \left(\sum_i e\sigma_i \delta(y - x_i) sg(x - y) \right) \tag{47}$$

$$= e \sum_i \sigma_i \int_0^L dy \left(\delta(y - x_i) sg(x - y) \right) \tag{48}$$

$$= e \sum_i \sigma_i sg(x - x_i) \tag{49}$$

$$= e \sum_{i|x_i<x} \sigma_i - e \sum_{i|x_i>x} \sigma_i \tag{50}$$

It's clear that the most likely low-temperature configurations of such a system are configurations where opposite charges are close together, as this minimizes the energy in the electric field. In addition, pairs of opposite charges emit no electric field outside of themselves. This is the motivation behind thinking of the two-component Coulomb plasma as a dielectric gas.

The physics of the system greatly depends on the background field θ. Consider $\theta = 0$. As discussed, we expect positive and negative charges to be grouped together. These pairs of charges move around without interacting with other pairs of charges. As such, they behave like a gas.

Now consider what happens as we increase θ slowly. The (-,+) pairs have the electric field between them weakened, whereas the (+,-) pairs have it strengthened. Thus, we might expect that in the most likely configuration, there is still a dielectric gas, but (-,+) pairs are favored or (+,-) pairs have a shorter average distance between them.

When the field takes value $\theta = e$, (-,+) pairs dissociate, because the field between them is 0, and the system resembles a plasma. We can track this dissociation in the potential energy $U_{\theta,L}$. In this scenario, $2q = \theta = e$. Consider the potential energy of two charges, σ_1, σ_2 with $\sigma_1 = -1 = -\sigma_2$ and $x_1 < x_2$. Then the potential energy of this system becomes independent of the separation between the charges.

$$U_{L,\theta} = e^2|x_1 - x_2| - e^2(-x_1 + x_2) + \theta^2 L/4 \tag{51}$$

$$= e^2|x_1 - x_2| - e^2|x_1 - x_2| + \theta^2 L/4 = \theta^2 L/4 \tag{52}$$

At $\theta = 2e$, we have charges e and $-e$ at 0 and L. The field can be screened by the generation of a negative charge at 0 and a positive charge at L. The same total-screening effect can occur at

any even multiple of the charge $\theta = 2ke, k \in \mathbb{Z}$. Thus, the dynamics of the system are periodic in θ, with period $2e$ [13].

2.4.2 Equivalence of the two-component Coulomb plasma to the particle in a periodic potential

When we discussed the Schwinger model, we saw how the system of interacting fermions is equivalent to a system of bosons. A similar thing occurs in its ostensible classical equivalent, the two-component Coulomb plasma. In this subsection, we will see how the partition function for a particle in a periodic potential is equivalent (up to constant factors) to the partition function for the system here [13].

The grand-canonical partition function $Z(\theta, L)$ is found by integrating not only over the degrees of freedom of the system (particle positions and parities) but also summing over the particle number, which in general is not fixed. Suppose that we are working in the section of phase space where the total charge is neutral i.e. $\sum \sigma_i = 0$. Then we can take $2N$ to be the number of particles, N of them having parity +1 and N having -1. For simplicity, let the first N have parity +1 and the next N have parity -1, and let z be the "cost" of creating a particle $e^{\beta\mu}$. Then

$$Z(\theta, L) = \sum_{N=0}^{\infty} \frac{z^{2N}}{N!N!} \int dx_1 ... dx_{2N} e^{-\beta U_{L,\theta}(x_1 ... x_{2N})} \tag{53}$$

where the x_i are each integrated over $[0, L]$. The reason we have the factor $1/(N!)^2$ is because the first N particles are all indistinguishable from each other. The same is true for the last N particles.

The corresponding grand-canonical pressure [13] is

$$p(\beta, \theta) = \lim_{L\to\infty} \frac{1}{L\beta} \log Z(\theta, L) \tag{54}$$

Consider the Matthieu Hamiltonian for a particle in a periodic potential, with $D = 2\beta e^2$ and z the chemical potential from before:

$$H = \frac{1}{2} D p^2 - 2z \cos x \tag{55}$$

We will show that the partition function for this Hamiltonian in the limit $T \to 0$ is equal, up to constant factor, to the partition function for the two-component Coulomb plasma in the case of zero external field. To get the corresponding Hamiltonian when $\theta \neq 0$, we add $\theta/2e$ to the momentum before squaring.

The partition function for a Hamiltonian with a discrete number of energies is $\sum e^{-\beta E} = \operatorname{Tr} e^{-\beta H}$. We can compute the trace in position space, naming the inverse temperature parameter L instead of β for reasons that will become apparent.

Now, suppose that we write e^{-LH} as $(e^{-\epsilon H})^N$ where $\epsilon = L/N$, for some positive integer N. Since H commutes with itself, this is allowed. Then, suppose we insert the identity operator between each

$e^{-\epsilon H}$. We will eventually take the limit as $\epsilon \to 0$ and recover an integral over paths from 0 to L.

$$\begin{aligned} Z &= \int dx_0 \langle x_0| e^{-LH} |x_0\rangle \\ &= \int dx_0 \langle x_0| e^{-\epsilon H} ... e^{-\epsilon H} |x_0\rangle \\ &= \int dx_0 dx_1 ... dx_{N-1} \langle x_0| e^{-\epsilon H} |x_1\rangle \langle x_1| e^{-\epsilon H} |x_2\rangle ... \langle x_{N-1}| e^{-\epsilon H} |0\rangle \end{aligned}$$

Note that $e^{-\epsilon H}$ can be decomposed, because $\epsilon H = \frac{1}{2} D\epsilon \hat{p}^2 - 2z\epsilon \cos\hat{x}$, therefore, the commutator of its individual terms goes like $\epsilon^2(\sin\hat{x}\hat{p} + \hat{p}\sin\hat{x})$, which disappears in the limit as $\epsilon \to 0$. Thus, we can rewrite $e^{-\epsilon H}$ as $e^{-\frac{1}{2}D\epsilon\hat{p}^2} e^{2z\epsilon\cos\hat{x}}$, and then we can introduce the identity operator (this time taken in momentum space) to compute $\langle x_0| e^{-\epsilon H} |x_1\rangle$ as an integral.

$$\begin{aligned} [\frac{1}{2} D\epsilon\hat{p}^2, -2z\epsilon\cos\hat{x}] &= -zD\epsilon^2 [\hat{p}^2, \cos\hat{x}] \\ &= -zD\epsilon^2([\hat{p}, \cos\hat{x}]\hat{p} + \hat{p}[\hat{p}, \cos\hat{x}]) \\ &= -zD\epsilon^2 i\{\sin\hat{x}, \hat{p}\} \to 0 \end{aligned}$$

$$\begin{aligned} \langle x_0| e^{-\epsilon H} |x_1\rangle &= \langle x_0| e^{-\frac{1}{2}D\epsilon\hat{p}^2} e^{2z\epsilon\cos\hat{x}} |x_1\rangle \\ &= \int dp \langle x_0| e^{-\frac{1}{2}D\epsilon\hat{p}^2} |p\rangle \langle p| e^{2z\epsilon\cos\hat{x}} |x_1\rangle \\ &= \int dp \langle x_0| e^{-\frac{1}{2}D\epsilon p^2} |p\rangle \langle p| e^{2z\epsilon\cos x_1} |x_1\rangle \\ &= \int dp e^{-\frac{1}{2}D\epsilon p^2} e^{2z\epsilon\cos x_1} \langle x_0|p\rangle \langle p|x_1\rangle \\ &= \frac{1}{2\pi} e^{2\epsilon z\cos x_1} \int dp e^{-\frac{\epsilon}{2}Dp^2 + ip(x_0 - x_1)} \\ &= \frac{1}{\sqrt{2\pi D\epsilon}} e^{2z\epsilon\cos x_1 - \frac{\epsilon}{2D}(\frac{x_0 - x_1}{\epsilon})^2} \end{aligned}$$

$$Z = \int dx_0 ... dx_{N-1} \left(\frac{1}{2\pi D\epsilon}\right)^{N/2} e^{\sum_{i=1}^{N-1}(2z\cos x_i - \frac{1}{2D}p_i^2)\epsilon} \tag{56}$$

where $p_i \equiv (x_i - x_{i-1})/\epsilon$ and x_N is identified with x_0. Although the integral is highly divergent, since the factor on the outside blows up to infinity, we can just label the factor as a constant and move on. One justification for this is that all physically relevant quantities that we want to measure from the partition function are given by derivatives of $\log Z$, and any factor C of Z will separate into $\log C + \log Z$, and then would be differentiated out.

One interesting thing to notice is that, if p_i is very large, or equivalently if $|x_i - x_{i+1}| >> \epsilon$, then the sum would be very negative, and so the exponential would take a very small value. Thus, when integrating over the degrees of freedom $x_0 ... x_{N-1}$, the dominating regions of the domain of

the integral will be where x_i is very close (order ϵ or even closer) to x_{i-1} and x_{i+1}. This motivates thinking of the sequence $x_0, x_1 ... x_{N-1}, x_0$ as a closed path, $x(\tau)$. The sum in the exponential suggests that τ goes from 0 to $N\epsilon = L$. Integrating over the degrees of freedom is now equivalent to integrating over all paths $x(\tau)$ that begin and end at the same point. Thus, the way to interpret the partition function in this limit is as a path integral.

$$Z = C \int Dx(\tau) e^{\int_0^L d\tau (2z \cos x(\tau) - \frac{1}{2D}(dx/d\tau)^2)} \tag{57}$$

We require $p(\tau)$ to be well-defined at every point i.e. $x(\tau)$ is at-least differentiable once. One natural restriction is that the path $x(\tau)$ is smooth i.e. all derivatives $x^{(n)}(\tau)$ exist on the interval $\tau \in [0, L]$. Thus the first derivative is continuous. Furthermore, because the starting point for the path is arbitrary (we could have started the path from any x_i, because it is cyclic), another sensible restriction is also requiring $x^{(n)}(0) = x^{(n)}(L)$ for all n i.e. the paths are not only closed, but smooth and periodic in τ with period L. Now, if we do integration by parts on the momentum term, we get that $\int_0^L -(dx/d\tau)^2 d\tau = \int_0^L x(d^2x/d\tau^2) d\tau$.

$$Z = C \int Dx(\tau) e^{\int_0^L d\tau (2z \cos x(\tau) + \frac{1}{2D} x(d^2x/d\tau^2))} \tag{58}$$

We note that the above integral is left invariant by certain transformations on the integrating variable $x(\tau)$. For example, if we replace $Dx(\tau)$ with $D(-x(\tau))$, the space of paths we are integrating over is invariant, and likewise the exponential is left invariant too. Likewise, adding a constant to the path, i.e. $Dx(\tau) \to D(x(\tau) + c)$, must also leave the integrating space invariant.

We can also expand the above integral in powers of z, using the series formula for e^x. In order to expand the integral in powers of z, we need to be able to compute $(\int_0^L 2\cos x(\tau) d\tau)^n$. We can rewrite cosine in the terms of complex exponentials and simplify further using the fact that the coefficients should be left invariant by one of the previously mentioned transformations. Integrals that seem dependent on the added constants **must** be identically zero.

$$Z = \sum_{n=0}^{\infty} \frac{z^n C}{n!} \int Dx(\tau) e^{\int_0^L d\tau (\frac{1}{2D} x(d^2x/d\tau^2))} \left(\int_0^L 2\cos x(\tau) d\tau \right)^n \tag{59}$$

$$\begin{aligned} \left(\int_0^L 2\cos x(\tau) d\tau \right)^n &= \int_0^L d\tau_1 (e^{ix(\tau_1)} + e^{-ix(\tau_1)}) ... \int_0^L d\tau_n (e^{ix(\tau_n)} + e^{-ix(\tau_n)}) \\ &= \int_{[0,L]^n} d\tau_1 ... d\tau_n \sum_{(\sigma_1 ... \sigma_n) \in \{-1,1\}^n} e^{i \sum_{i=1}^n \sigma_i x(\tau_i)} \end{aligned}$$

If we plug in this form for the nth power of the integral into the equation for Z, we will get multiple terms, one for each of the 2^n possible bit-vectors $(\sigma_1, ... \sigma_n)$. However, if $\sum_i \sigma_i \neq 0$, then after the transformation $x(\tau) \to x(\tau) + c$, there will be a factor of $e^{ic \sum_i \sigma_i}$. The integral over

momentum is left unchanged. Thus, except for when c is a multiple of 2π, this will change the value of the coefficient for the z^n term. This suggests that the terms where $\sum_i \sigma_i \neq 0$ must be integrated out. This significantly reduces the number of non-trivial terms! Now, n must be even and we have only have $\binom{n}{n/2}$ non-trivial terms for each power of n in the expansion. If we label the set of bit-vectors who have an equal number of -1's as 1's as $\mathcal{S}$, the partition function now takes the form

$$Z = \sum_{n \text{ even}} \frac{z^n C}{n!} \sum_{(\sigma_1 \ldots \sigma_n) \in \{-1,1\}^n | \sum_i \sigma_i = 0} \int_{[0,L]^n} d\tau_1 \ldots d\tau_n \int Dx(\tau) e^{(\int_0^L d\tau \frac{1}{2D} x(d^2x/d\tau^2)) + i \sum_i \sigma_i x(\tau_i)} \tag{60}$$

$$= \sum_{n \text{ even}} \frac{z^n C}{n!} \sum_{(\sigma_1 \ldots \sigma_n) \in \mathcal{S}} \int_{[0,L]^n} d\tau_1 \ldots d\tau_n \int Dx(\tau) e^{\int_0^L d\tau (\frac{1}{2D} x(d^2x/d\tau^2) + i x(\tau) \sum_i \sigma_i \delta(\tau - \tau_i))} \tag{61}$$

The integral over $Dx(\tau)$ can be evaluated using the identity [14]

$$\int Dx(\tau) e^{\int d\tau - \frac{1}{2} x \hat{A} x + iJx} \propto e^{-\frac{1}{2} \int \int d\tau d\tau' J(\tau) P(\tau - \tau') J(\tau')} \tag{62}$$

where P is the corresponding propogator for the differential operator $\hat{A}$, satisfying $\hat{A}P(x-y) = \delta(x-y)$. For the integral we are concerned with, $J = \sum_i \sigma_i \delta(\tau - \tau_i)$, $\hat{A}$ is $\frac{-1}{D} \frac{d^2}{d\tau^2}$, and it can be easily verified that the corresponding propogator is $P(\tau) = -D \max(0, \tau)$. Let B be the constant of proportionality. Furthermore, since we integrate over all the degrees of freedom simultaneously, it doesn't matter what the actual bit vector $(\sigma_1, \ldots \sigma_n)$ is. We can replace the sum with a $\binom{n}{n/2}$, and take the first $n/2$ σ to be positive and the rest negative.

$$Z = \sum_{n \text{ even}} \frac{z^n CB}{n!} \sum_{(\sigma_1 \ldots \sigma_n) \in \mathcal{S}} \int_{[0,L]^n} d\tau_1 \ldots d\tau_n e^{\frac{D}{4} \int \int d\tau d\tau' \sum_j \sigma_j \delta(\tau - \tau_j) \max(0, \tau - \tau') \sum_i \sigma_i \delta(\tau' - \tau_i)} \tag{63}$$

$$= CB \sum_{n \text{ even}} \frac{z^n}{n!} \sum_{(\sigma_1 \ldots \sigma_n) \in \mathcal{S}} \int_{[0,L]^n} d\tau_1 \ldots d\tau_n e^{\frac{D}{4} \sum_{i,j} \sigma_i \sigma_j \max(0, \tau_j - \tau_i)} \tag{64}$$

$$= CB \sum_{n \text{ even}} \frac{z^n}{n!} \sum_{(\sigma_1 \ldots \sigma_n) \in \mathcal{S}} \int_{[0,L]^n} d\tau_1 \ldots d\tau_n e^{\beta e^2 \sum_{j=1}^n \sum_{i<j} \sigma_j \sigma_i |\tau_j - \tau_i|} \tag{65}$$

$$= CB \sum_{n \text{ even}} \frac{z^n}{(n/2)!^2} \int_{[0,L]^n} d\tau_1 \ldots d\tau_n e^{\beta e^2 \sum_{j=1}^n \sum_{i<j} \sigma_j \sigma_i |\tau_j - \tau_i|} \tag{66}$$

$$= CB \sum_{N=0}^{\infty} \frac{z^{2N}}{N!N!} \int_{[0,L]^{2N}} d\tau_1 \ldots d\tau_{2N} e^{-\beta U_{L,0}(\tau_1, \ldots \tau_{2N})} \quad \blacksquare \tag{67}$$

Since the two-component Coulomb plasma has the same partition function as the particle in a periodic potential, we can compute all of the thermodynamic quantities of the former by using the latter. In particular, we can compute the dielectric constant κ in the thermodynamic limit, and get $\kappa = \beta\theta^2/3\epsilon_0(\theta/2e)$, where ϵ_0 is the energy of the first band of the Matthieu Hamiltonian

[13]. This value is bounded, and so this provides further justification to think of the two-component Coulomb plasma as a dielectric gas. If the gas were a plasma, then any induced electric field would be screened, and so the dielectric constant would be infinite [13].

3 Localization

Localization is a phenomenon in quantum systems where system fail to thermalize. Single-particle localization, or Anderson localization, is a phenomenon where single particle wave-functions for lattices with short-range self-interactions remain localized (in position-space) if disorder is added to the system [15]. Many-body localization is localization in the many-body eigenstates of the Hamiltonian [16].

Many-body localization stands in opposition to thermalization of quantum many-body systems. Systems that localize do not thermalize. Thermalization is associated with the spreading of information via entanglement, known as *decoherence*. Thus, if we examine a subset of a large quantum system, the expectation values of observables in the thermalizing limit approach the thermal equilibrium values, and thus initial, local information is lost. This does not happen in many-body localized states.

3.1 Anderson Localization

Anderson localization applies to lattice systems of arbitrary dimension with a short-range self-interaction potential (i.e. the components of the single-body wavefunction can interact with eachother). As an introductory exercise we can consider the dynamics of a system where a single quantum particle hops around (in position-space) on a one-dimensional lattice. We can add disorder to this Hamiltonian via a random on-site potential, $V(n) \in [-\theta, \theta]$. The first term is known as the tight-binding model. It describes electron hopping in metals [17].

$$H = -t \sum_n (c_n^\dagger c_{n+1} + c_{n+1}^\dagger c_n) + \sum_n V(n) c_n^\dagger c_n \tag{68}$$

In the case of no-disorder, after an infinite amount of time, we expect that a particle initially in a spatially localized wave-packet is equally likely to be anywhere on the lattice. Correspondingly, the single-body wave function spreads out in position-space. However, a miraculous thing happens when we add disorder: single-body wave-functions remain localized in position-space, even after arbitrary long amounts of time. Furthermore, the amount of disorder is *irrelevant* for one-dimensional and two-dimensional lattices. This phenomenon is known as Anderson localization.

We can see in the glimmer of this phenomenon in the above Hamiltonian. Consider an arbitrary single-body state $|\psi\rangle$.

$$|\psi\rangle = \sum_n \psi(n) c_n^\dagger |0\rangle \tag{69}$$

$$H|\psi\rangle = = \left(-t\sum_n (c_n^\dagger c_{n+1} + c_{n+1}^\dagger c_n) + \sum_n V(n) c_n^\dagger c_n\right) \sum_n \psi(n) c_n^\dagger |0\rangle$$
$$= \left(-t\sum_n (c_n^\dagger \psi(n+1) + c_{n+1}^\dagger \psi(n)) + \sum_n V(n)\psi(n) c_n^\dagger\right)|0\rangle$$

Suppose now that $|\psi\rangle$ is a single-body eigenstate of the Hamiltonian with energy ϵ. Eigenstates of the Hamiltonian have trivial time-evolution as they only get scaled by a phase factor. Therefore, if $|\psi\rangle$ is an energy eigenstate, its position-space probability distribution is constant as a function of time. With strong enough disorder, we can show that the single-body energy eigenstates are localized in position-space. Thus, if $|\psi\rangle$ is initially localized on a site n, it will be close to an energy eigenstate, and thus it will not spread out with time.

$$\epsilon\psi(n) = -t(\psi(n-1) + \psi(n+1)) + V(n)\psi(n) \tag{70}$$

In the limit where t is very small, this eigenvalue equation can be satisfied with $\psi(m) \approx 1$ with energy $\epsilon \approx V(m)$. That is to say, if t is small, the wave-function for a particle sitting on one site doesn't evolve with time (i.e. localizes) because it is an energy eigenstate, and has energy equal to the random potential on which it is sitting. Anderson proved that this phenomenon happened in arbitrary dimension for a sufficiently strong disorder strength[2]. For a infinite lattice system with short-range (say, nearest neighbor) interactions and a random on-site potential, the expected deviation of a particle is bounded, i.e.

$$\sum_{n\in\mathbb{Z}^d} |\psi(t,n)|^2 |n| \leq C \tag{71}$$

for some positive constant C [15].

A wave function that spreads out uniformly in time violates this inequality. For example, consider a wave-function that spreads out uniformly on a line, e.g. at time $t = T$, $|\psi(n)|^2 = 1/(2T+1)$ for $|n| \leq T$ and $|\psi(n)|^2 = 0$ elsewhere, for $T = 0, 1, 2$ and so on. Then the expected deviation $\sum_{n\in\mathbb{Z}} |\psi(t,n)|^2|n| = \frac{1}{2T+1} 2(1+2+...T) = \frac{T(T+1)}{2T+1}$ is unbounded in T. Anderson showed that this sort of "spreading out" of the wave-function is forbidden for a large-class of disordered, single-body Hamiltonians.

Put another way, the presence of disorder prevents the particle from delocalizing. This is why an electron in a metal with impurities will stay in one place compared to an electron in a metal without impurities. In short, impurities stop waves [15].

[2]For $d = 1, 2$, θ can be arbitrary, but for $d \geq 3$, localization happens if $\theta/\hbar$ is sufficiently big.

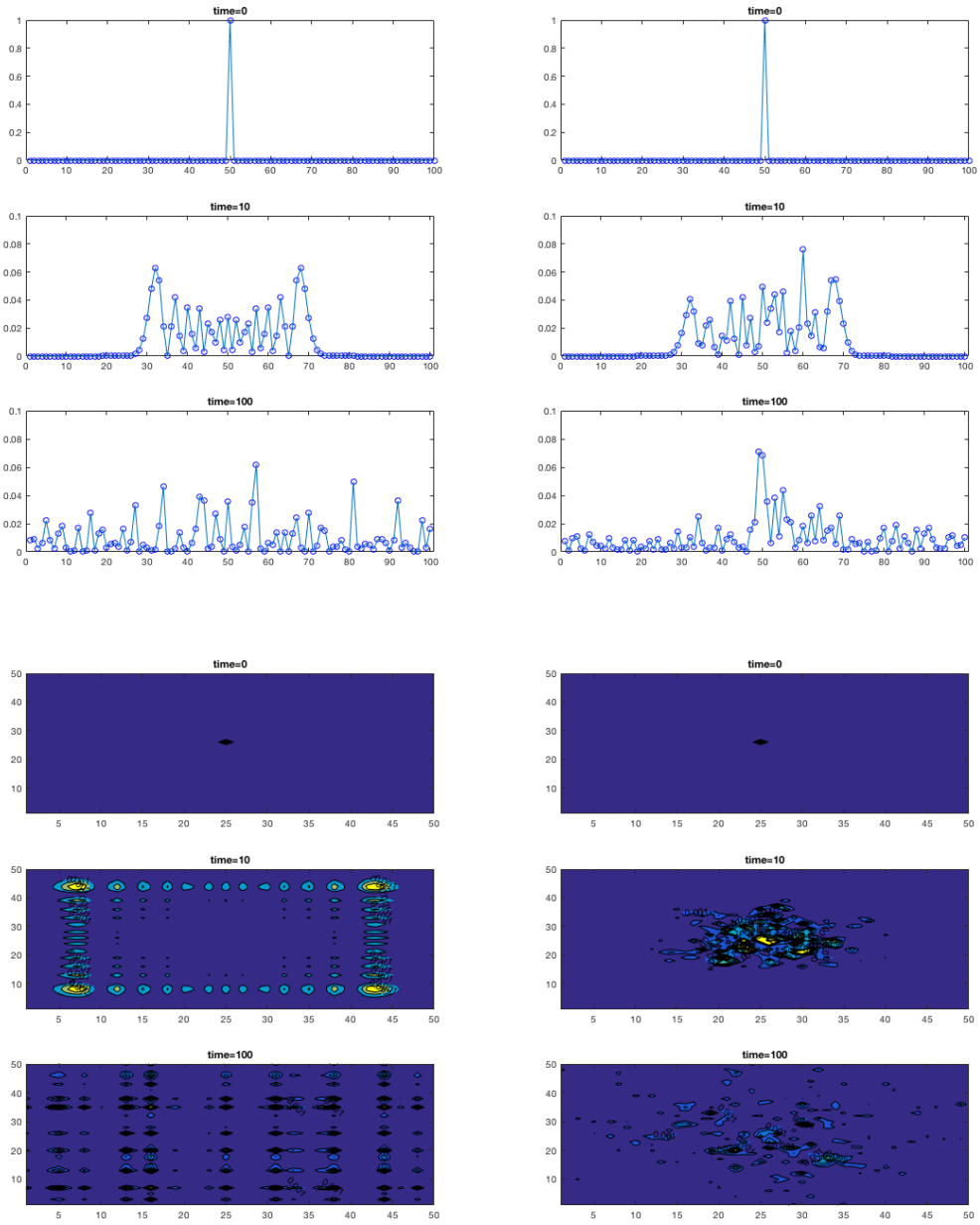

Figure 7: The first set of figures show the time evolution of a single-body state in the hopping system with disorder discussed above. For $\theta = 0$, we see that the wave-function spreads out in position space and looks fairly evenly spread. For $\theta = 0.5$, we see that the wave-function still remains localized at the point at which it starts. We also look at the 2D equivalent of the first model. As we can see for $\theta = 0$, it is unlocalized, whereas for $\theta = 2$, it remains localized.

3.2 Many-Body Localization

Although Anderson localization only involves the single-body states of the Hamiltonian, there can be localization in the many-body states as well [18], [19]. Many-body localization is a property of interacting Hamiltonians with disorder where the many-body eigenstates are localized or uncorrelated. [16] suggests a definition of many-body localization (MBL) where a system is said to many-body localize if it fails the Eigenstate Thermalization Hypothesis (ETH). The Eigenstate Thermalization Hypothesis is that all energy eigenstates of a system are thermal i.e. if a system starts off in an energy eigenstate, and we examine a small section of the system, then the expectation values of all observables for this small section equal their thermodynamic average [16]. In essence, the subsystem decoheres with its surroundings, and information about its initial conditions is lost. In MBL, like single-body localization, the presence of disorder prevents this decoherence.

Pure quantum systems evolve unitarily, and so are reversible and no information is lost. However, suppose we restrict our attention to a subsystem A of the full system, $A \otimes B$. A system thermally equilibrates when it's able to act as a bath for every small subsystem. When this happens, the reduced density matrix for the subsystem goes to the Gibbs state with the degrees of freedom outside the sub-system traced out, $\mathrm{Tr}_B\, e^{-\beta H}/Z$, in the large-reservoir limit. If the density matrix for *every* subsystem A goes to the Gibbs state with the extra d.o.f. traced out (in the limit where B is infinitely big and $t \to \infty$), the system is said to be thermal. When a system fails to act as a reservoir, it localizes [16]. However, entanglement still spreads in many-body localized states from non-entangled initial conditions, but at a logarithmic rate. Furthermore, the many-body localized eigenstates obey area-law entanglement as opposed to volume-law, which is seen in thermalized eigenstates [16]. This area-law entanglement gives rise to an efficient matrix product state representation, because the bond dimension can be kept small.

Intuitively, long-range interactions should prevent the wave function from localizing in position space. If there's a long-range interaction, even a long-range hopping in the single-body case, that means that components of the wave-function that are far away from each other in position space can be correlated. Thus, long-range interactions help the wave-function spread out or decohere, working against localization. Similarly, they suggest that area-law entanglement should no longer hold. This is because such interactions provide a mechanism by which all of the sites in a sub-region can become entangled with sites outside the region. Since many-body localized states obey area-law entanglement scaling, this suggests that a system with long-range interactions cannot localize. The Schwinger model, therefore, is expected to thermalize.

A more precise argument of why long-range interactions kill localization is presented in [9]. They consider the general two-body spin Hamiltonian of spin 1/2 particles on a d-dimensional lattice with a random on-site disorder ϵ_i chosen uniformly from $[-W, W]$. The Hamiltonian contains a hopping term with strength $t_{ij}/|r_{ij}|^{\alpha}$ between sites i, j and a density-density interaction term with strength

$V_{ij}/|r_{ij}|^\beta$. Physically, hopping can't persist farther than density-density interactions so $\beta \leq \alpha$. Note that the discretized Schwinger model is indeed an example of the matrix above, since each squared E-field term can be expanded into a sum of two-body terms.

$$H = \sum_i \epsilon_i S_i^z - \sum_{ij} \frac{t_{ij}}{|r_{ij}|^\alpha}(S_i^+ S_j^+ + h.c.) + \sum_{ij} \frac{V_{ij}}{|r_{ij}|^\beta} S_i^z S_j^z \tag{72}$$

The authors place limits on many-body localization by asking whether the expected number of resonant pairs, or pairs of sites through which energy can be transported via swapping spins, diverges as a function of distance on the lattice. A resonant pair is where $|\epsilon_i - \epsilon_j| \lesssim t_{ij}/|r_{ij}|^\alpha$. Suppose we fix some site i and look at the number of resonant pairs j it has s.t. $R_1 < |r_{ij}| < 2R_1$. If the disorder is chosen randomly from $[-W, W]$, site j is a resonant pair with i with probability $\frac{t_{ij}}{R_1^\alpha W}$. Since the probability that distinct sites j, j' are resonant pairs with i is independent (we assume the ϵ_i are chosen independently), the expected number of resonant pairs in the region goes like $R^d \frac{t_{ij}}{R_1^\alpha W}$. This quantity diverges if $d > \alpha \geq \beta$. Thus, for sufficiently long-range interactions, such as the one in the Schwinger model where $\beta = -1$, we expect MBL to fail [9]. Still, the bosonized version is *short*-ranged, which sets up the puzzle this thesis tries to solve.

3.3 A Brief Overview of Random Matrix Theory

When the single-body Hamiltonian localizes, its energies become the random potentials added to each site. Thus, the distribution of energies would be uniform, with mean zero, and the energy density is Poisson distributed. By contrast, delocalized states exhibit spectral properties captured by random matrix theory. Here we examine the distribution of random orthogonal matrices, or the Gaussian Orthogonal Ensemble (GOE). In the GOE, we see *level repulsion*, where matrices whose the energy levels are close are significantly less likely. Furthermore, we see *spectral rigidity*, where there is little fluctuation in the density of eigenstates in a given energy interval [20].

The Wigner-Dyson distribution describes the GOE, which is an ensemble of random, real-symmetric matrices on which we define a probability measure that is orthogonally invariant (i.e. $P(H) = P(Q^T H Q)$ for orthogonal Q). In this ensemble, the matrix elements on or above the diagonal are chosen from a probability distribution f, and the remaining elements are determined by symmetry. If we require that the random matrix elements of a given matrix H in this ensemble are statistically independent and identically distributed, then $P(H) = \prod_{i \leq j} f(H_{ij})$ where f is the probability distribution of the elements of H. It can be shown that these two conditions on $P(H)$ (orthogonal invariance and that the matrix elements are independently chosen from the same distribution) imply that f must be Gaussian [21].

$$P(H) \propto \exp(\frac{-1}{4\sigma^2} \operatorname{Tr}(H^2)) \tag{73}$$

This probability measure is clearly orthogonally invariant, since the Trace is orthogonally invariant i.e. $\mathrm{Tr}((Q^THQ)^2) = \mathrm{Tr}(Q^TH^2Q) = \mathrm{Tr}(H^2)$. One can use this distribution to derive the Wigner surmise, which describes level repulsion[3]. The distribution of eigenvalues for GOE matrices is

$$P(E_1, E_2...E_N) \propto \prod_{i<j} |E_i - E_j| \exp\left(-\frac{1}{4\sigma^2}\sum_k E_k^2\right) \tag{74}$$

Note that the order in which the eigenvalues appear in the matrix is irrelevant, since symmetric matrices with the same eigenvalues are related to each other via orthogonal transformation. The Wigner-Dyson distribution has been shown to accurately predict the statistical properties of spectra of large atomic nuclei, and in fact, was initially studied to understand their spectra [21].

The predictive power of the Gaussian Orthogonal Ensemble is not limited to the spectra of large atomic nuclei. It has been adapted to a describe the statistical properties of many large, disordered, time-reversal invariant quantum systems[4]. In fact, it was conjectured by Bohigas, Giannoni, and Schmit that "spectra of time-reversal-invariant systems whose classical analogs are K systems show the same fluctuation properties as predicted by GOE." That is to say, quantum systems with T-symmetry whose classical analogs are chaotic display level repulsion and spectral rigidity in their spectra [20].

3.4 Measures of Localization

We have established that in single-body localized systems, the spectrums behave quite differently from the GOE. We now present a measure on the spectrum of a random matrix that carries two vastly different values for localized matrices, where the energies are distributed uniformly on some interval, and GOE matrices: the level statistics ratio.

Recent literature suggests that the level statistics is an effective measure of localization [18]. The level statistics ratio $< \tilde{r} >$ is a number that is associated with the spectrum of a random matrix. One computes $< \tilde{r} >$ for random matrix A as follows:

1. Compute the spectrum $\{E_i\}$ of A, with $E_0 \leq E_1... \leq E_{N-1}$.
2. Define the gap vector S by $S_i = E_{i+1} - E_i$. Note that S has $N-1$ elements.
3. Define the vector $\tilde{r}$ by $\tilde{r}_i = \min(S_{i+1}, S_i)/\max(S_{i+1}, S_i)$. Note that this vector has $N-2$ elements.
4. The level statistics ratio is the mean of $\tilde{r}$.

The level statistics ratio has a number of important properties. Firstly, the level statistics ratio is invariant of the basis representation, since it is only a function of the eigenvalues i.e. $< \tilde{r} >$

[3]The Wigner surmise can be easily derived for a 2x2 symmetric matrix, as shown in [22].

[4]Time-reversal invariance in Hamiltonians implies they have an real-symmetric representation.

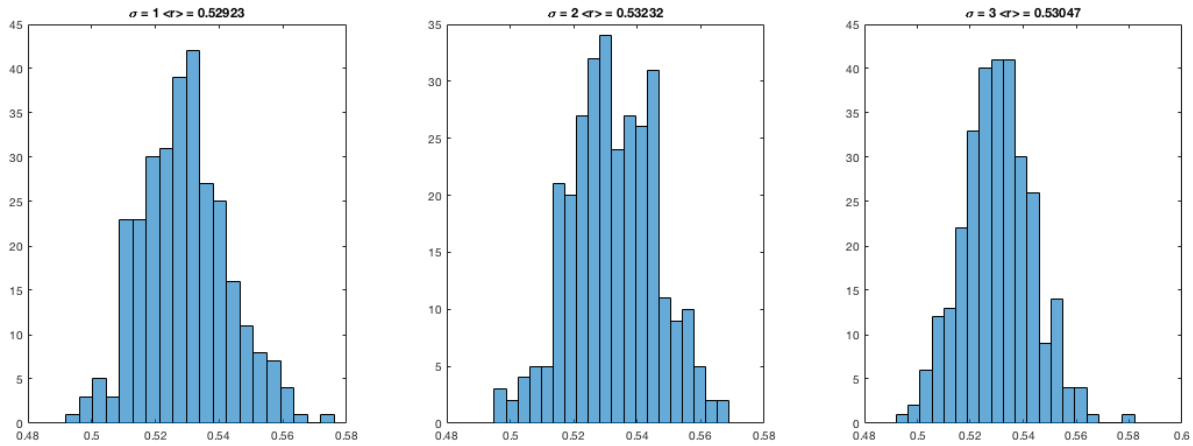

Figure 8: The level statistics ratio is averaged over 300 500×500 matrices from the GOE, and the level statistics ratio of each one is presented as a histogram. Changing the standard deviation σ seems to have little effect on the level statistics ratio.

$(A) =< \tilde{r} > (Q^T A Q)$, where Q is orthogonal. The level statistics ratio is also invariant under linear transformations on A i.e. $< \tilde{r} > (A) =< \tilde{r} > (\alpha A + \beta \mathbb{I})$. The latter relation is easy to see, since

$$A \to \alpha A + \beta \mathbb{I} \implies E_i \to \alpha E_i + \beta$$

and β drops out in step (2) and α drops out in step (3). If the level statistics ratio was not independent of constants added to the Hamiltonian, or scaling the Hamiltonian, it would be of little interest for assessing whether a system many-body localizes.

Unsurprisingly, the level statistics ratio is highly dependent on the distribution of the eigenvalues of A. For large, GOE matrices, where the elements are chosen from the normal distribution of mean 0 and variance 1, we get a drastically different value for $< \tilde{r} >$ than if the eigenvalues themselves were distributed uniformly. Furthermore, the level statistics ratio is independent of σ for GOE matrices at large N, as the figure suggests.

$$\boxed{< \tilde{r} >_{GOE} = 0.5314 \qquad < \tilde{r} >_{poisson} = 0.3836} \tag{75}$$

If the energy eigenvalues are uniformly distributed in some interval, then the energy density follows a Poisson distribution. Thus, if the matrix in study was an element of the GOE and large, its level statistics ratio would be close to 0.5314, but if the energies were chosen uniformly, its level statistics ratio would be close to 0.3836.

For the Anderson-localized, single-body block of the disordered Hamiltonian, the level statistics ratio should approach the latter of the two numbers presented, regardless of disorder strength. This is because the energies become uniformly distributed. Note that the length of the energy interval is irrelevant, since scaling the spectrum doesn't change the level statistics ratio.

For many-body localized systems, we also expect that the level statistics ratio in the localized eigenstates will be close to the Poisson value [23]. This is because the localized energy eigenstates are weakly correlated. In the localized regime, level-repulsion and spectral rigidity disappear, and so the spectrum will no longer resemble the GOE.

The aim of this paper is to probe the disordered massless Schwinger model for MBL. We will assess localization via the level statistics ratio. It is hypothesized that in the lowest energy density states in the weak interaction regime, we will see the level statistics ratio approach the Poisson value, because that is the regime in which bosonization is valid and the system of interacting fermions is equivalent to a system of non-interacting bosons.

4 The Random Massless Schwinger Model

4.1 The Argument for MBL in the Bosonized Schwinger Model

We present the argument for MBL in the continuum bosonized massless Schwinger model with disorder, found in [24].

The exact bosonized representation of the massless Schwinger model is given in terms of a bosonic field ϕ and corresponds to the free massive boson scalar field. The first term is the free scalar field and the second term is the pinning or mass term. Both terms are given straightforwardly from the bosonization dictionary. We add the disorder term H_{dis}, already bosonized, directly to the bosonized Hamiltonian H. We can imagine that adding disorder either scatters the fermions backwards, sending left-movers to right-movers and vice versa, or it scatters forwards, sending left-movers to left-movers and right-movers to right-movers. The scattering terms are multiplied by random Gaussian variables $\eta(x)$ for forward-scattering and $\xi(x)$ for backward-scattering. The disorder term also contains the UV cutoff α, which bounds the momentum of the fermions we are examining.

$$H = \int \frac{dx}{2\pi} v_F[\pi^2\Pi^2(x) + (\nabla\phi(x))^2 + \frac{4e^2}{2\pi^2}\phi^2(x)] \tag{76}$$

$$H_{dis} = -\int dx[\frac{1}{\pi}\eta(x)\nabla\phi(x) + \left(\frac{\xi^*(x)}{2\pi\alpha}e^{i2\phi(x)} + h.c.\right)] \tag{77}$$

If we make the substitution $\phi(x) \to \phi(x) - \frac{1}{v_F}\int^x dy\eta(y)$, we see that the first term in the disorder integral only contributes an additive constant. Furthermore, we can substitute $\xi^*(x)$ for $\xi^*(x)e^{\frac{2i}{v_F}\int^x dy\eta(y)}$, which is also a Gaussian distributed random variable. Thus, the full, disordered, bosonized Hamiltonian (up to additive constant) is

$$H = \int \frac{dx}{2\pi} v_F[\pi^2\Pi^2(x) + (\nabla\phi(x))^2 + \frac{4e^2}{2\pi^2}\phi^2(x)] + \int dx \left(\frac{\xi^*(x)}{2\pi\alpha}e^{i2\phi(x)} + h.c.\right) \tag{78}$$

We also rewrite $\xi(x) = D(x)e^{i\xi(x)}$ in terms of independent random variables $D(x)$ and $\xi(x)$ with short-range correlations. Adding disorder has the effect of shifting the equilibrium positions for the ground state in the 1d crystal corresponding to the free massive scalar boson. The new energy-minimizing field configuration $\phi_0(x)$ can be solved by minimizing the Hamiltonian above. We can write the Hamiltonian in terms of field $\delta\phi(x) \equiv \phi(x)$ which represents the difference between the field and the minimum energy configuration.

$$H = \int dx v_F\pi^2\Pi^2(x) + v_F(\nabla\phi)^2 + [\frac{4e^2}{\pi} - \frac{2D(x)}{\pi\alpha}\cos(2\phi_0 - \xi)]\phi^2 + O(\phi^3) \tag{79}$$

At leading order, this describes gapped bosons in a random potential, which is known to have all its single-particle eigenstates localized [24]. The higher-order terms are also short-ranged in real-space, and thus the bosonized, disordered, massless Schwinger model in 1d should many-body localize [24].

4.2 Mapping to Spin Model

The randomized massless Schwinger model includes a random on-site potential $V(n)$ chosen uniformly from $[-\theta, \theta]$. In the fermion language, the Hamiltonian is

$$H = \frac{-i}{a^2 g^2} \sum_n (\phi_n^\dagger e^{i\theta_n} \phi_{n+1} - h.c.) + \sum_n V(n) \phi_n^\dagger \phi_n + \sum_n L_n^2 \tag{80}$$

After Jordan-Wigner, solving or L_n and dropping constant terms, we get the randomized, massless Schwinger model in the spin language in terms of parameters $N, l_0, x, \lambda, \theta$:

$$H = x \sum_{n=0}^{N-2} \left(\sigma_n^+ \sigma_{n+1}^- + \sigma_n^- \sigma_{n+1}^+\right) + \lambda \sum_{n=0}^{N-2} \left(l_0 + \frac{1}{2} \sum_{k=0}^{n} \left(\sigma_k^z + (-1)^k\right)\right)^2 + \sum_{n=0}^{N-1} \frac{1}{2} V(n) \sigma_n^z \tag{81}$$

This is the model we are using for numerical analysis.

4.3 Parameter Regimes of Interest

As we discussed earlier, bosonization only occurs where the dispersion is linear or approximately linear. Therefore, any perturbation to the hopping term near the Fermi energy must be small. If $x = 1.0$ and consists of $O(N)$ terms and there are $O(N^2)$ interaction terms, then in the bosonization regime, it must be the case that λa is $O(1/N)$, where a is the lattice constant. But since $a = 1$ in our numerics, we have λ be $O(1/N)$. If θ were sufficiently big, we would get Poisson statistics trivially. The disorder should be less than the hopping strength x in order to have meaningful results, so $\theta < 1/2$. Furthermore, we restrict $x >> \lambda >> \theta$, since the proof for long-range interactions killing MBL used that the disorder potential was bigger than the interaction potential. Since the argument for MBL in the bosonized Schwinger model was made on the continuum and our numerics were done on a lattice, finite size effects are relevant, but it is unclear how to measure them.

4.4 A Brief Summary of Implementation

We are using an exact diagonalization approach to generate the full or partial spectrum for massless Schwinger Hamiltonians with disorder. Since $< \tilde{r} >$ is itself a random variable for a given set of parameters, we take multiple samples of the spectrum for the same parameters. As expected, the level statistics ratio stabilizes the more we increase N, since increasing N by two roughly quadruples the size of the Hamiltonian.

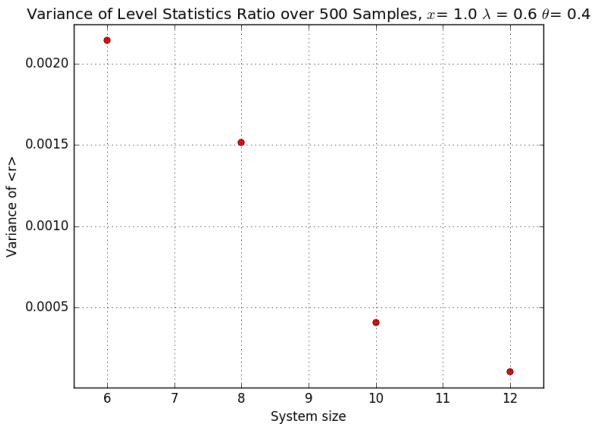

Figure 9: Here we see the variance in $< \tilde{r} >$ over $m = 500$ samples, as a function of N for a given assignment of the parameters. The level statistics ratio stabilizes over larger matrices.

A natural basis for computation is the basis defined by the local σ^z operators. In this basis, the action of σ_n^z, $\sigma_n^\pm$ is easily programmable. We can rewrite the interaction term as a linear combination of such operators acting on two sites at once.

$$H = x \sum_{n=0}^{N-2} \left(\sigma_n^+ \sigma_{n+1}^- + \sigma_n^- \sigma_{n+1}^+\right) + \lambda \left(\sum_{n=0}^{N-1} s(n) \sigma_n^z + \sum_{j=1}^{N-2} \sum_{i=0}^{j-1} \frac{1}{2} k(j) \sigma_i^z \sigma_j^z \right) + \sum_{n=0}^{N-1} \frac{1}{2} V(n) \sigma_n^z \quad (82)$$

where $s(n)$ is a vector which is a function of l_0, and $k(j)$ is independent of the parameters. This form of the Hamiltonian can be straight-forwardedly derived and is left out for brevity.

To minimize memory-use, we represent each vector of the fixed total-spin subspace as a bit-vector. It's clear the value of total z-spin $\frac{1}{2}\sum_n \sigma_n^z$ fixes the number of zeros and ones, and so we can write a simple recursive method to generate the basis states without repetition. We order the basis states in reverse-alphanumeric order, thus 0 (1) is mapped to $|-1\rangle$ ($|+1\rangle$) eigenvector of σ^z.

We can now construct the Hamiltonian directly in this basis as a $n \times n$, sparse matrix, where $n = \binom{N}{N/2}$ in the total-spin zero case. We construct the Hamiltonian in $O(Nn \lg n)$ time, making use of the fact that any bitvector $|j\rangle$, there are at most $O(N)$ $|i\rangle$ s.t. $\langle i| H |j\rangle$ is non-zero[5]. For each bitvector $|j\rangle$, we compute the possible $|i\rangle$ s.t. $\langle i| H |j\rangle$ is non-zero, and to determine what row in the matrix each $|i\rangle$ corresponds to takes $\lg n$ time using a simple binary search in the basis.

Since we don't construct the full Hamiltonian, we are only using $O(Nn)$ memory, which is far superior to actually constructing the full $n \times n$ matrix. Furthermore, this is much more efficient than constructing the full $2^N \times 2^N$ Hamiltonian first, then projecting into the total-spin zero subspace.

There are a number of things we do to speed up the implementation. For the largest systems

[5]If one uses a dictionary and defines a straightforward hash function, one could reduce the time complexity to $O(Nn)$, but construction only happens once per site and is not a bottleneck of the algorithm.

we consider, we use Lanczos algorithm to compute a small subset of the full spectrum. Lanczos algorithm is optimized for hermitian matrices and computing only the largest eigenvalues [25]. We also speed up calculating disorder realizations for a given set of parameters by subtracting off the old disorder and adding the new disorder in. This greatly speeds up the implementation because we aren't constructing a new Hamiltonian for each sample, just modifying the existing one in memory. We also make use of multiple CPUs and cores via the Feynman cluster. The calculation of the level statistics ratio can be broken up into independent processes, one for each evaluation of the parameters. For the largest system sizes, we also parallelize each disorder realization.

We examine the level statistics ratio for $\lambda = 0.125$, for the clean system $\theta = 0$ and at weak disorder strengths $\theta = 0.01, 0.02, 0.05$. The system sizes we consider are $N = 12, 14, 16, 18$. We sample over 400 disorder realizations for $N = 12$, 200 for $N = 14$, and then 100 for $N = 16$ and $N = 18$. We average over fewer disorder realizations for larger system sizes for two reasons: first, because the running time for generating the spectrum for larger system sizes increases quite rapidly, and second, because the level statistics ratio stabilizes as we increase system size. For $N = 18$, one disorder realization could take as long as 5-6 hours. The 300 disorder realizations we generated for $N = 18$ would have been impossible to produce if we did not parallelize on the cluster.

4.5 Results

4.5.1 The clean system

We begin the results by presenting the data for the clean system, where there is no disorder. First we examine the crystalline behavior as a function of λ. When there is no interaction, $\lambda = 0$, there is no preferred spin direction, and so the equilibrium spin on each site is 0. At low temperatures, as we turn up λ, we see crystalline modes appear. This makes sense because the lowest energy state for the interaction term, which corresponds to the vacuum, has this structure. Thus, as λ grows, we expect the expectation values for the local z-spin to approach ± 1.

The high-temperature limit we see a different structure emerge. Firstly, as expected the expectation values are much smaller in magnitude. Secondly, where before we saw that the even (odd) sites had negative (positive) expectation values, here we only see the general trend that the spin gradually increases going left to right on the lattice. This effect also occurs in the low-temperature case. This is because of the explicit symmetry-breaking introduced by the alternating background charge.

We also include numerical evidence for the emergence of a gap as we turn on the interaction. The presence of a gap is in agreement with the results of [1], the fact that the system has an efficient matrix product state representation for the ground state, and the argument for MBL in the bosonized Schwinger model, which suggests that the system behaves like gapped bosons. The results suggest that even as the system size grows, any excitation to the ground state on the lattice will have some

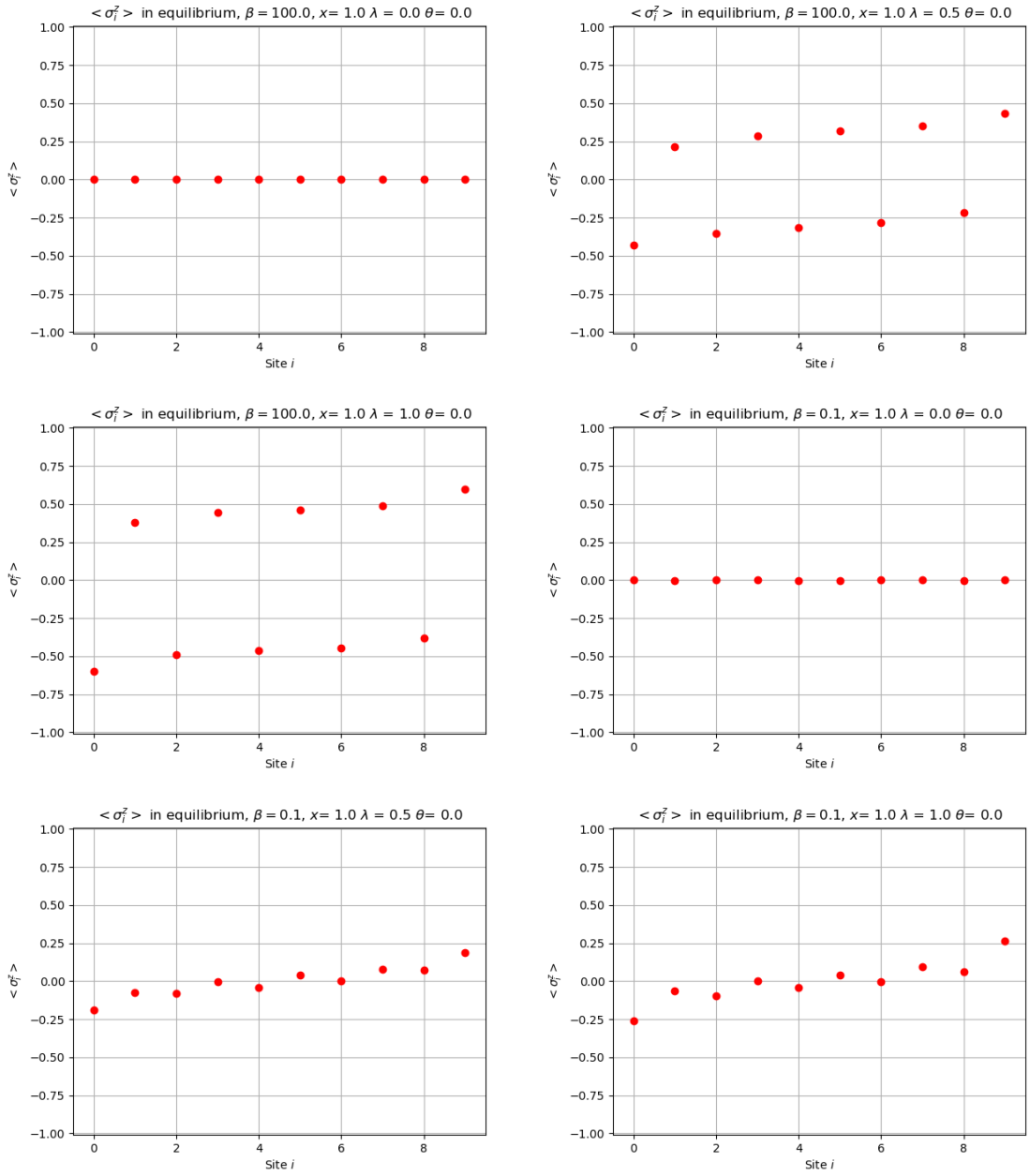

Figure 10: The thermodynamic equilibrium values for the spin on each site for $N = 10$ and no disorder. We vary both temperature β^{-1} and interaction strength λ.

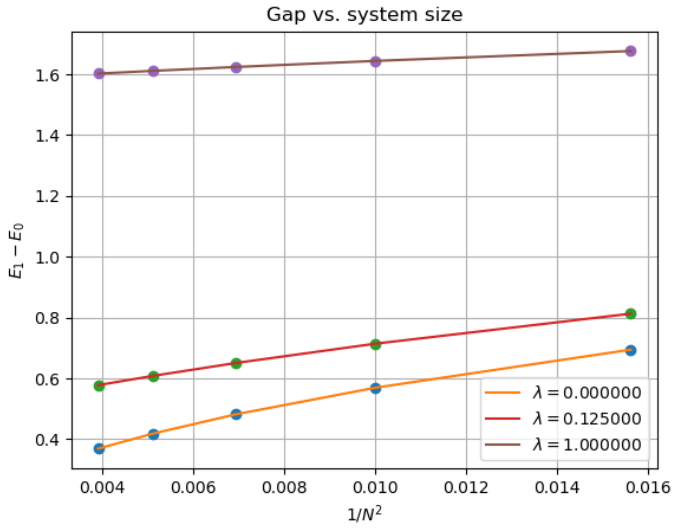

Figure 11: We look at the gap vs interaction strength. For no interaction and no disorder, we expect the gap to go to zero because we should only have the cosine dispersion. As we increase the interaction, we see the concavity change and the presence of a gap emerge.

small, finite energy cost. The interaction-less case, on the other hand, has a $\cos k$ dispersion, which in the continuum limit $N \to \infty$, presents no gap.

In agreement with the argument for MBL in the bosonized Schwinger model, the clean system shows integrability in the lowest energy states. This is evidenced by the level-statistics ratio over the first 100 energies having the Poisson value at the largest system sizes. Additionally, we examine the level crossings for the first 100 energies. According to the Bohigas conjecture, non-integrable systems obey Wigner-Dyson statistics. Therefore, because of level repulsion, as we vary λ, the energy levels of the matrix should not cross if the system is non-integrable. Our results show that energy levels do cross at $\theta = 0$ and also at small disorder, suggesting that the system is integrable at $\theta = 0$.

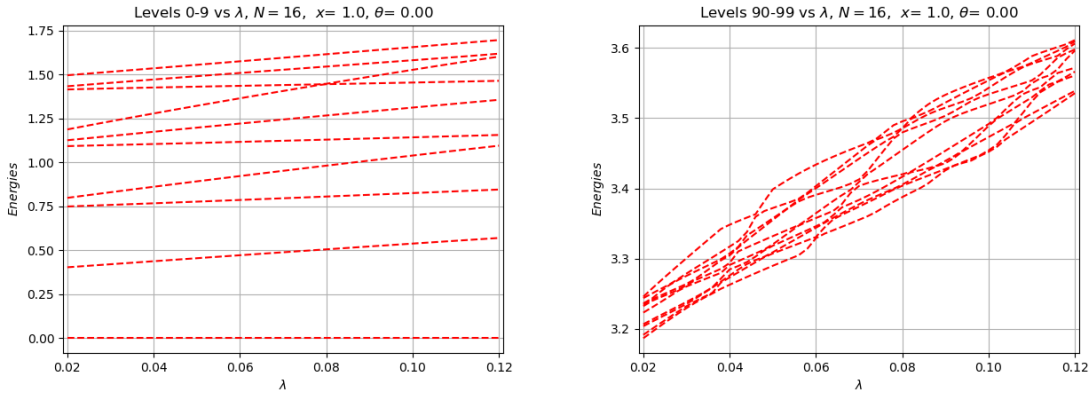

Figure 12: We present the level crossings for the 10 lowest and 10 highest levels for the first 100 energies of the clean model, $N = 16, \lambda = 0.125, x = 1.0, l_0 = 0$.

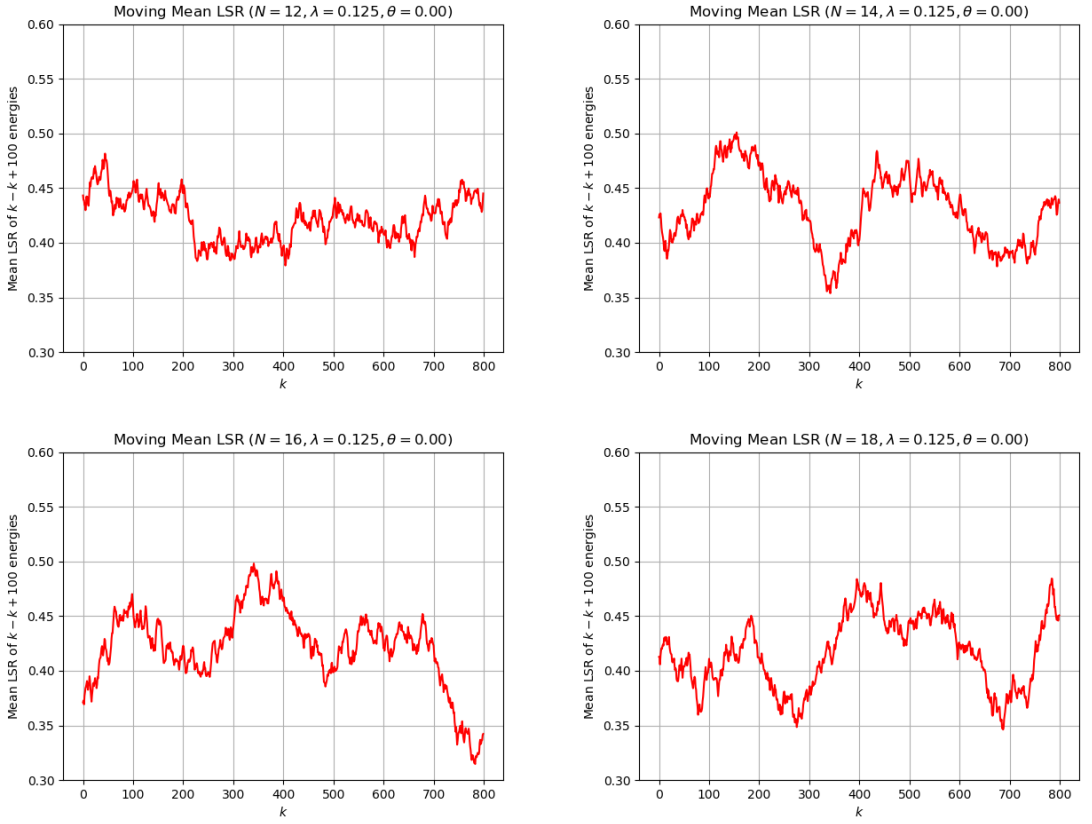

Figure 13: Each data point represents the level-statistics ratio over 100 consecutive energies. We see that for the first 100 energies, and for other chunks of the spectrum, the level statistics ratio approaches the Poisson value, pointing to the integrability of the clean system. It is puzzling as to why, even in the clean system, $< \tilde{r} >$ does not vary smoothly with k. More analysis is needed to explain this behavior.

4.5.2 The disordered system

The evidence presented in this section supports the argument that the massless Schwinger model many-body localizes in the regime where $x >> \lambda >> \theta$. The strongest example is found in $N = 16$, where the lowest energy states take Poisson value or are very close to the Poisson value. The level statistics ratio has non-negligible variance over the different disorder realizations, so we plot the mean level statistics ratio over the different realizations with the corresponding error bars.

Furthermore, at low energies, the variance in $< \tilde{r} >$ settles down compared to high energies. This can be seen directly in the plot with the error bars, which are smaller for smaller values of k. Additionally, although the total mean level statistics ratio should stabilize for larger system sizes because we are taking an average over more $\tilde{r}$ values, we have roughly the same sized error bars for all system sizes. However, this could be because we are looking at a much smaller fraction of the spectrum of $N = 16$ and $N = 18$. In any case, $< \tilde{r} >$ does not vary smoothly with k, even in the clean system. More analysis is needed in order to have a clear explanation of why this is the case.

If θ is much larger than the interaction, then as predicted by the argument against localization in long-range many-body interacting systems, the level-statistics ratio should not be near Poisson. We test the argument presented in [9] by looking at a moving average of the level-statistics ratio for $\theta = 1.0$ and $\lambda = 0.1$ for $N = 16$. At all energy levels, we see that the mean level statistics ratio for the moving average is roughly constant for each consecutive 100 levels, and takes a value near the GOE average.

The highest energy levels in the bosonization parameter regime are still delocalized. This effect is somewhat noticeable for $N = 12$ since there are only 924 energy levels total in that system, so we are actually observing the level statistics ratio over segments of the whole spectrum. However, even at $N = 16$ and $N = 18$, we see the trend that $< \tilde{r} >$ for the higher energy states goes towards the GOE value. This also serves as more evidence for the bosonization argument in [24], since the argument only predicts MBL is the lowest energy states.

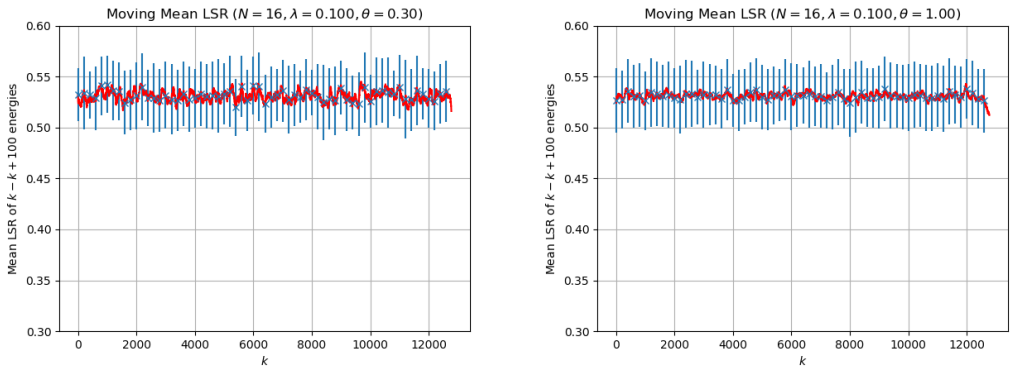

Figure 14: For $\theta >> \lambda$, the level statistics ratio goes to the GOE average at all energy densities, as predicted by the arguments against MBL in long-range interacting systems.

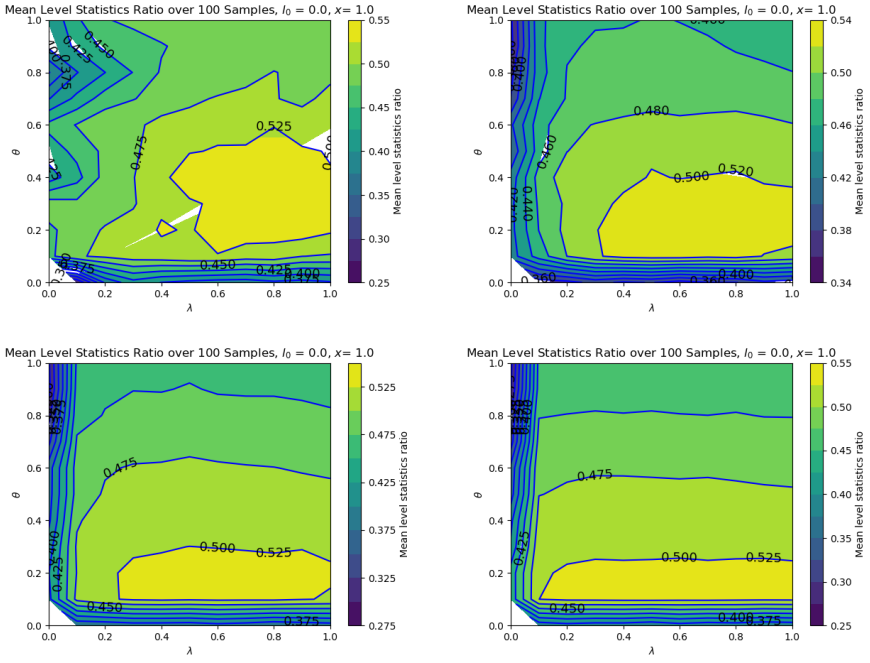

Figure 15: Here we see the a contour graph of the mean level statistics ratio (over all levels) for system sizes of $N = 8, 10, 12$ and 14. For each parameter configuration, the level statistics ratio is averaged over 100 samples.

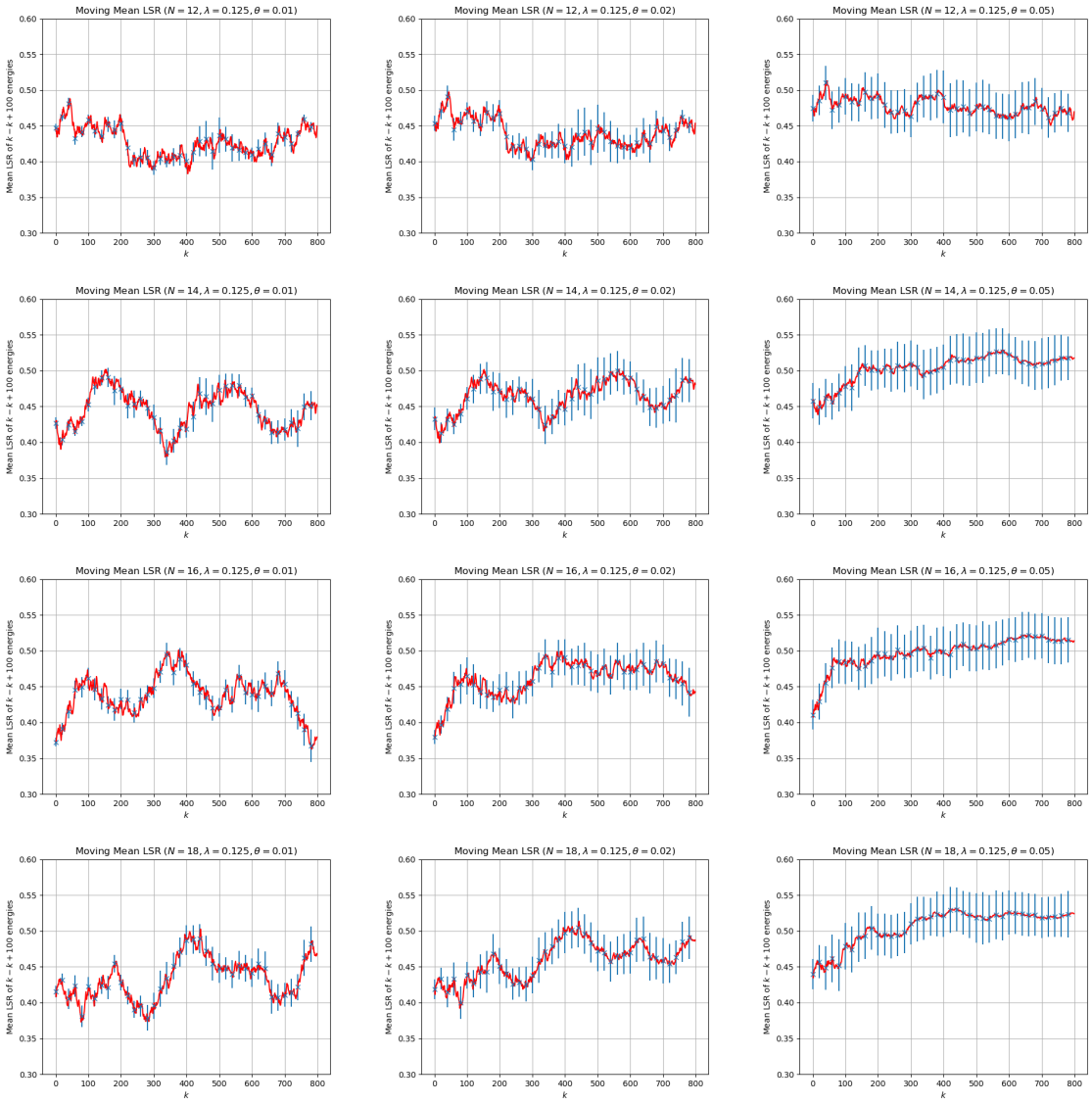

Figure 16: Each row is a different system size, $N = 12, 14, 16, 18$ and each column is a different amount of disorder $\theta = 0.01, 0.02, 0.05$. The y-axis ranges from 0.3 to 0.6. As we increase system size and decrease finite size effects, we see that the lowest 100 energies of the model have Poisson statistics in the presence of disorder. We argue that this is evidence of many-body localization in favor of the argument presented at the beginning of this chapter. The red curve represents the mean level statistics ratio averaged over the corresponding number of disorder realizations. The blue error bars are given by the standard deviation of the distribution which is being averaged over to get the red curve.

4.6 Conclusion

This thesis provides strong numerical evidence to in favor of many-body localization in the massless Schwinger model. This is a remarkable result since the Schwinger model has long-range interactions, and MBL is generally understood to be killed by long-range interactions in the regime where disorder is much stronger than kinetic energy. Using bosonization, we argue that MBL can exist at low energies. Our numerical evidence supports the analytic argument for localization in the massless Schwinger model in a very different regime than in [9]. Here, x is much greater than λ which is much greater than θ.

Many-body localization is of general foundational interest for quantum statistical mechanics and is also promising for quantum memory. Learning more about the scenarios in which MBL can manifest is vital to many in the field. In the spirit of [16], can we use this added property of MBL to create stable quantum memory? After all, since MBL stands in opposition to thermalization, information about initial conditions are not washed out, and decoherence, the usual impediment to stable quantum memory, is defeated. A large number of physical systems have inherent long-range interactions which were previously thought to exclude any possibility of MBL. However, the numerical simulations presented in this paper suggest that MBL can occur even in systems with long-range interactions, giving some credence to the idea.

The result of this paper also provides some explanation as to why the massless Schwinger model has an efficient matrix product state representation for the ground and low-lying excited states [1]. The low-bond dimension suggests that the entanglement entropy obeys area law, which is a property of many-body localized states. MBL in systems with long-range interactions is therefore promising for efficient tensor network representations.

Another natural question is how the results of this section might differ if instead we used the alternative formulation presented in section two. Would the results be different? If so, what would that suggest about the one-component Coulomb plasma?

There are various ways to improve the results of this paper. One option is to sample more disorder realizations for the data presented. Although the number of disorder realizations was chosen so that the variance in the level statistics ratio was small, one can make it smaller by having more disorder realizations. Although we only presented the level statistics ratio for one value of λ, we found similar results with different values of the interaction strength; future studies can present this data as well. One can also give more precise numerical evidence for why Poisson statistics are not just the result of integrability in the system. In addition, future studies will need to better understand the finite-size effects and their role in the numerics. Since the arguments in [24] generalize to higher dimensions, future studies can also explore localization in systems with two or more spatial dimensions.

References

[1] M. C. Bañuls, K. Cichy, K. Jansen, and J. I. Cirac, "The mass spectrum of the Schwinger model with Matrix Product States," *JHEP*, vol. 11, p. 158, 2013.

[2] M. Peskin and D. Schroeder, *An Introduction to Quantum Field Theory*. Westview Press, 1995.

[3] M. Stone, *The Physics of Quantum Fields*. Springer, 2012.

[4] J. D. Hunter, "Matplotlib: A 2d graphics environment," *Computing In Science & Engineering*, vol. 9, no. 3, pp. 90–95, 2007.

[5] The Mathworks, Inc., Natick, Massachusetts, *MATLAB version 9.0.0.341360 (R2016a)*, 2016.

[6] J. Taylor, *Classical Mechanics*. University Science Books, 2002.

[7] R. Shankar, "Bosonization: How to make it work for you in condensed matter," *Acta Phys. Polon.*, vol. B26, pp. 1835–1867, 1995.

[8] E. Miranda, "Introduction to bosonization," *Brazilian Journal of Physics*, vol. 33, pp. 3 – 35, 03 2003.

[9] N. Y. Yao, C. R. Laumann, S. Gopalakrishnan, M. Knap, M. Müller, E. A. Demler, and M. D. Lukin, "Many-body localization in dipolar systems," *Phys. Rev. Lett.*, vol. 113, p. 243002, Dec 2014.

[10] J. B. Kogut and L. Susskind, "Hamiltonian Formulation of Wilson's Lattice Gauge Theories," *Phys. Rev.*, vol. D11, pp. 395–408, 1975.

[11] C. Henley, "Fermion operators and hopping bands." Lecture notes from Cornell, 2009.

[12] Wikipedia, "Jordan-wigner transformation — wikipedia, the free encyclopedia," 2009. [Online; accessed 9-April-2017].

[13] J. Bernasconi and T. Schneider, eds., *One-Dimensional Coulomb Systems*, vol. Physics in One Dimension: Proceedings of an International Conference, (Fribourg, Switzerland), August 1980.

[14] Wikipedia, "Common integrals in quantum field theory — Wikipedia, the free encyclopedia." `http://en.wikipedia.org/w/index.php?title=Common\%20integrals\%20in\%20quantum\%20field\%20theory&oldid=752089635`, 2017. [Online; accessed 30-April-2017].

[15] P. W. Anderson, "Absence of diffusion in certain random lattices," *Phys. Rev.*, vol. 109, pp. 1492–1505, Mar 1958.

[16] R. Nandkishore and D. A. Huse, "Many body localization and thermalization in quantum statistical mechanics," *Ann. Rev. Condensed Matter Phys.*, vol. 6, pp. 15–38, 2015.

[17] Wikipedia, "Hubbard model — Wikipedia, the free encyclopedia." `http://en.wikipedia.org/w/index.php?title=Hubbard\%20model&oldid=776177371`, 2017. [Online; accessed 29-April-2017].

[18] A. Pal and D. A. Huse, "Many-body localization phase transition," *Phys. Rev. B*, vol. 82, p. 174411, Nov. 2010.

[19] D. M. Basko, I. L. Aleiner, and B. L. Altshuler, "On the problem of many-body localization," *eprint arXiv:cond-mat/0602510*, Feb. 2006.

[20] O. Bohigas, M. J. Giannoni, and C. Schmit, "Characterization of chaotic quantum spectra and universality of level fluctuation laws," *Phys. Rev. Lett.*, vol. 52, pp. 1–4, Jan 1984.

[21] Y.-K. Liu, "Statistical behavior of the eigenvalues of random matrices," 2001.

[22] L. D'Alessio, Y. Kafri, A. Polkovnikov, and M. Rigol, "From quantum chaos and eigenstate thermalization to statistical mechanics and thermodynamics," *Advances in Physics*, vol. 65, pp. 239–362, May 2016.

[23] M. Serbyn and J. E. Moore, "Spectral statistics across the many-body localization transition," *Phys. Rev. B*, vol. 93, p. 041424, Jan 2016.

[24] R. Nandkishore, A. Akhtar, S. Sondhi, and M. C. Banuls, "Many body localization with long range interactions." Will be published at later date.

[25] Wikipedia, "Lanczos algorithm — Wikipedia, the free encyclopedia." `http://en.wikipedia.org/w/index.php?title=Lanczos\%20algorithm&oldid=773773892`, 2017. [Online; accessed 01-May-2017].

This paper represents my own work in accordance with University regulations.

Ahmed Akhtar